Volume 4 – Earthquake Seismology

Dynamic Triggering

David P. Hill
U.S. Geological Survey
345 Middlefield Rd. Menlo Park, CA 94025, USA

Stephanie G. Prejean
U.S. Geological Survey
Alaska Volcano Observatory
Anchorage, AK 99508, USA

Revisions complete as of 9/5/06

Accepted for publication in *Treatise on Geophysics* (G. Schubert, ed.), Chapter 8 in Volume **4**, "Earthquake Seismology" (H. Kanamori, ed.)

Related Chapters: 3, 4, 5, 7, 11 in Volume 4

Volume 4 – Earthquake Seismology

Dynamic Triggering

Contents

ABSTRACT

A growing body of evidence demonstrates that dynamic stresses propagating as seismic waves from large earthquakes are capable of triggering additional earthquakes ranging from aftershocks in the near-field (within one or two source dimensions of the mainshock epicenter) to remotely triggered earthquakes at distances exceeding 10,000 km. Most of the triggered earthquakes are small (generally $M \leq 3$) except within the near-field where dynamic stresses may trigger slip on subadjacent fault segments leading to complex rupture comprised of several large earthquakes of comparable magnitude. Crustal surface waves with periods of 15 to 30 seconds and peak dynamic stresses greater than ~0.01 MPa seem to be most efficient in triggering remote seismicity. Current models for dynamic triggering fall under two broad groups -- one appealing to Coulomb failure with various friction laws and the other appealing to the activation of crustal fluids either hydrous or magmatic. No single model appears capable of accounting for the wide variation observed in the nature of triggered activity. Spatial sampling of dynamic triggering on a global scale is still woefully inadequate because of the limited distribution of adequate seismic networks. From the limited data currently available, it appears that extensional stress regimes hosting geothermal and volcanic activity are more susceptible to remote dynamic triggering than compressional stress regimes, although remote triggering is not limited to extensional regimes. Instances of remote triggering in the few areas with continuous, high-resolution deformation instrumentation (all volcanic or geothermal areas) include distinctive deformation transients, suggesting that the locally triggered seismicity in these area may be a secondary response to a more fundamental, aseismic process that likely involves some form of fluid transport or phase change. Recent evidence for triggering by solid Earth tides and ocean loading in convergent plate margins provides a low-frequency, low-amplitude reference point for the spectrum of stresses capable of dynamic triggering. Remaining challenges include establishing better sampling of the distribution of triggered seismicity and better constraints on physical models for the triggering process.

8.01 INTRODUCTION

One of the outstanding questions in earthquake seismology involves the nature of short-term processes that ultimately trigger slip on a given fault. The Earth's crust is pervasively laced with faults, and multiple lines of evidence indicate that the brittle crust is in some sense critically stressed and in a state of incipient failure nearly everywhere (Zoback and Zoback 2002). Because long wavelength stresses associated with the relative motion of major tectonic plates accumulate relatively slowly (rates of ~10^{-5} MPa per year or less), regional stresses may remain incrementally below the frictional strength of faults (typically on the order of ~10 to 100 MPa) for periods of decades to centuries. Insight into the triggering question thus depends on understanding the influence of short-term, short-wavelength fluctuations in both the stress field and fault strength, such that the local stress state temporarily exceeds the local failure threshold leading to slip nucleation and an earthquake.

Sources of short- to mid-term stress fluctuations in the crust are many. Those most likely to be significant at seismogenic depths include: 1) other earthquakes in the crust (Das and Scholz 1981, Freed 2005, Steacy et al. 2005, Harris 1998), 2) magmatic intrusions (Savage and Clark 1982, Hill et al. 2002, Manga and Brodsky 2005), 3) anthropogenic activities such as reservoir-filling, mining, and fluid injection or withdrawal (McGarr et al. 2002), 4) solid earth tides and ocean loading (Cochran et al. 2004), and 5) seasonal meteorological factors such as snow loading and ground water recharge (Christiansen et al. 2005). Local fluctuations in fault strength may result from changes in fluid pore pressure within a fault-zone (Lockner and Beeler 2002) , the nonlinear response of fault-zone friction to small perturbations in local stresses (Dieterich 1979, Johnson and Jia 2005), and sub-critical crack growth (Atkinson 1984).

In this chapter we are concerned with slip nucleation triggered either directly or indirectly by dynamic stress. Our principal focus will be on the evidence for triggering by dynamic stresses in the form of seismic waves (earthquake-earthquake interactions), but we also note recent evidence for tidal triggering as a quasi-static, low-amplitude reference point for the spectral range of oscillatory stressing with the potential for dynamic triggering. Because many sites displaying remotely triggered seismicity are volcanic and geothermal areas, our scope includes the response of magmatic and hydrothermal systems to dynamic stresses as potential sources for locally triggered seismicity. We conclude with a perspective on key challenges to be met in advancing understanding of dynamic triggering and its implications for active crustal processes.

8.01.1 Earthquake-Earthquake Interaction Modes

Earthquake-earthquake interactions in the form of mainshock-aftershock sequences have been recognized since the late 1800's and the emergence of seismology as a quantitative science (Omori 1894). With the global expansion of high-quality seismic networks coupled with the capabilities for resolving detailed spatial-temporal variations in deformation patterns afforded by satellite geodesy (continuous GPS and InSAR

technologies in particular), it has become increasingly clear that stress changes resulting from one earthquake are capable of triggering additional earthquake activity over a surprisingly wide range of distances and time scales. As currently understood, earthquake interactions are generally placed under one of three rather general stress transfer modes: 1) static, 2) quasi-static, or 3) dynamic.

8.01.1.1 Static and quasi-static stress triggering

Research on earthquake interactions associated with static stress triggering (the change in the static stress field from just before an earthquake to shortly after the dynamic stresses from the seismic waves have decayed away) began in the late 1960's and blossomed in the early 1990's with the growing availability of high-quality seismic and deformation data against which to test the patterns predicted by elastic dislocation models (Das and Scholz 1981, Harris 1998, King and Cocco 2001, Stein 1999). Shortly thereafter, extensions of the dislocation models were developed to account for gradual stress changes (quasi-static stress triggering) associated with viscous relaxation of the plastic lower-crust and upper mantle in response to the sudden dislocation (an earthquake) across a fault in the overlying brittle crust soon followed (Pollitz and Sacks 2002).

Both the static and quasi-stress interaction modes appeal to the permanent stress change produced by one earthquake nudging the stress field in the vicinity of a fault some distance away closer to the Coulomb failure threshold on that fault (e.g. Stein and Lisowski 1983, Hudnut et al. 1989, Harris 1998, Kilb et al. 2002, also see section 8.04 and Chapter 7). This concept is commonly expressed in terms of a change in the Coulomb Failure Function, or

$$\Delta CFF = \Delta\tau - \mu_s \Delta\sigma_n \quad (1$$

where

$$CFF = |\tau| - \mu_s \sigma_n - C \quad (2$$

is the Coulomb Failure Function, τ and σ_n are the shear and normal stress components acting on the fault, respectively, μ_s is the static coefficient of friction, and C is the cohesive strength (e.g. Oppenheimer et al. 1988, Harris 1998, Kilb et al. 2002, Cocco and Rice 2002, also see Chapters 3, 4, and 7). $CFF = 0$ corresponds to Byerlee's law for frictional failure (Byerlee 1980), and a positive change in CFF, or $\Delta CFF > 0$ indicates that the stress state has moved incrementally toward $CFF = 0$ and Coulomb failure.

Because static stress changes decay relatively rapidly with distance (as $\sim\Delta^{-3}$, where Δ is distance from the epicenter), their triggering potential is generally regarded as limited to one or two source dimensions from a given earthquake. Viscoelastic relaxation following a large crustal earthquake is largely confined to the lower crust and asthenosphere such that quasi-static stress changes propagate as a two dimensional stress change. Quasi-static stress changes thus decay more slowly with distance (as $\sim\Delta^{-2}$), their triggering potential thus extends to greater distances than static stress changes, and the relatively low visco-

elastic propagation speeds result in delayed triggering (Pollitz and Sacks 2002). These two interaction modes are the focus of Chapter 7 on stress transfer by G. King.

8.01.1.2 Seismic waves and dynamic stress triggering

The amplitudes of dynamic stresses propagating as seismic waves decrease relatively slowly with distance (as $\sim \Delta^{-2}$ for body waves and $\sim \Delta^{-3/2}$ for surface waves), and thus, their triggering potential extends from the near-field (the aftershock zone) to much greater distances than either the static or quasi-static stress changes as illustrated in Figure 1 (Kilb et al. 2000). Amplification by radiation directivity, which is not a factor in either static or quasi-static stress changes, can further enhance the amplitudes of dynamic stresses in a particular quadrant for earthquakes with unilateral fault rupture. Dynamic stresses are oscillatory, however, alternatively nudging the local stress field closer to and further from the local Coulomb failure stress over a range of frequencies leaving no permanent stress change. Indeed, it seems that Coulomb failure alone is not capable of explaining the full spectrum of observed dynamic triggering modes. In a number of cases, remotely triggered seismicity appears to be a secondary response to some more fundamental, aseismic process involving fluid activation or creep that was locally stimulated by the passing dynamic stresses.

<Figure 1 near here>

8.02 EVIDENCE FOR DYNAMIC TRIGGERING

Conceptually, dynamic triggering is based on the inference of a causal link between dynamic stresses (seismic waves) from a large earthquake propagating through a given site (event "*a*") and the onset of local earthquake activity at that site (event "*b*"). Credible evidence in support of such a causal link emerges with multiple, well-documented observations that event "*b*" follows event "*a*" within some "reasonable" time interval, Δt, (Figure 2). Statistical methods, if carefully formulated, can add backbone to malleable qualifiers such as "reasonable" and "sufficiently", thereby enhancing objective credibility of this inference when well posed tests indicate that the temporal sequence "*a*" then "*b*" cannot be dismissed as chance coincidences between random, statistically independent processes.

<Figure 2 near here>

A number of tests for the statistical significance of dynamic triggering appear in the literature, the most common of which is the β-statistic of Mathews and Reasenberg (1988). As an example, Figure 3 shows the β-statistic maps Gomberg et al. (2001) generated to evaluate patterns of dynamic triggering by the M_W = 7.4 1992 Landers and the M_W = 7.1 1999 Hector Mine earthquakes in southern California. Under this test, the value of β represents the number of standard deviations by which the seismicity rate during a specified time interval (two weeks in the case of Figure 3) following a dynamic stressing event exceeds an estimate of the background seismicity rate for a specified area. Values for $\beta > 2$ (two standard deviations) are generally considered to be statistically

significant. Here, it is important to note that many of the isolated areas that show up as red ($\beta > 2$) in Figure 3 do not correspond to areas of dynamic triggering from either the Landers or Hector Mine earthquakes. In Appendix I, we describe this test and its limitations when applied to dynamic triggering and provide references to alternative approaches. In essence, elevated β-statistics are permissive of dynamic triggering, but they are not sufficient by themselves to establish compelling statistical significance. They can, however, serve as a useful exploratory tool. This cautionary note underscores the importance of understanding the assumptions underlying any test for statistical significance and the implications inherent in the choice of parameters used in a specific the test

<Figure 3 near here>

8.02.1 Early Inferences on Dynamic Triggering

In an unpublished note dated 1955, Charles Richter wrote "*The reverse effect – a major earthquake triggering a minor shock – is most probably* [sic] *within the immediate aftershock are* [sic]*, but essentially by elastic wave propagation may set off action at a greater distance. If the distant effect is large enough, it may itself act as a trigger, so that there may be relay action, in which some of the later events are larger.*" (S. Hough, personal communication, 2005). Many of the early published inferences on dynamic triggering were associated with investigations into acoustic emissions and high-frequency seismic noise (see for example Armstrong and Stierman 1989, Nicolaev and Troitskii 1987 and references therein, Galperin et al. 1990) and concerns over the possibility that large, underground nuclear explosions might trigger a damaging earthquake (Emiliani et al. 1969). At the time, these studies were greeted within the scientific community by attitudes ranging from mild interest to strong skepticism. Skepticism prevailed largely because of questions regarding the statistical significance of isolated observations together with the lack of a compelling physical model. The fact that some of these studies were a part of efforts focused on even more controversial topics such as anomalous animal behavior induced by acoustic emissions as a means of earthquake prediction (e.g. Armstrong and Stierman 1989) probably contributed to the skeptical reception within the mainstream scientific community.

In the end, however, early investigations on dynamic triggering were hampered by limited data. The situation began changing with the rapid expansion of continuously recorded, telemetered seismic networks around the globe through the 1980's and 1990's coupled with improvements in real-time processing and a growing number of broad-band, high-dynamic-range digital installations set the stage for capturing a range of interesting seismic signals missed by the earlier instrumentation.

8.02.2 Widespread Evidence for Remote Dynamic Triggering in Western North America.

Between 1980 and the spring of 1992, four M~7 earthquakes shook the western United States including the M_W=7.4 Eureka, California earthquake of 8 November 1980 and the

M_W=7.1 Petrolia, California earthquake of 25 April 1992. Although many of the regional seismic networks were in place during this period, none of these earthquakes produced dynamic triggering that was noticed at the time.

8.02.2.1 The M_w = 7.4 Landers earthquake of 28 June 1992

On 28 June 1992, two months after the Petrolia earthquake, the M_w = 7.3 Landers earthquake ruptured a 70-km length of the Mojave Desert in southern California. Over the next few hours, it became clear that seismicity rates had increased at a number of sites across western North America at distances ranging from 200 to as much as 1,250 km (17 source dimensions). These sites included Long Valley caldera, Lassen Peak, Burney, CA, the Wasatch front in central Utah, Cascade Idaho, and Yellowstone National Park. Documented seismicity rate increases began within minutes to 33 hours following the Landers mainshock (Figures 2, 3, 4). This large number of independent occurrences provided overwhelming evidence that remote triggering by dynamic stresses is indeed a viable process in the Earth (Hill et al. 1993, Gomberg 1996).

<Figure 4 near here>

The Landers mainshock resulted from a unilateral rupture propagating to the north-northwest along a series of north-northwest striking dextral fault segments. All of the recognized sites of dynamic triggering were north of the Landers epicenter, suggesting that amplification enhanced by rupture directivity may influence the distribution of dynamic triggering – a suggestion borne out by subsequent instances of dynamic triggering (Gomberg et al. 2001). Indeed, the absence of notable triggering by the four earlier M~7 earthquakes may reflect the fact that they did not produce significant rupture directivity, or in the case of the M=7.4 Eureka earthquake of 1980, that rupture propagation was directed to the southwest away from the continental United States. With the notable exception of a M=5.6 earthquake beneath Little Skull Mountain in southern Nevada 240 km north of the Landers epicenter, the earthquakes triggered by Landers had magnitudes of M~3 or less with a tendency for the maximum magnitude to decrease with increasing distance for the Landers epicenter (Anderson et al. 1994).

All of the remote triggering occurred in areas of elevated background seismicity in transtensional tectonic settings. This was underscored, for example, by the absence of a triggered response along the creeping section of the San Andreas Fault through central California and Parkfield that, although a persistent source of small earthquakes, is a transpressional stress regime (Spudich et al. 1995). Many of the triggered sites were areas of geothermal activity and/or Quaternary volcanism (Hill et al. 1993, Anderson et al. 1994, Gomberg 1996)

8.02.2.2 The M_w 7.1 Hector Mine earthquake of 16 October 1999

On 16 October 1999, a M=7.1 earthquake ruptured a 40 km length of the Mojave Desert along a series of faults located just 20 km east of the Landers rupture (Figures 3, 4). In this case, fault rupture was bilateral but with the dominant rupture direction to the south-

southeast. The most energetic triggered response to the Hector Mine dynamic stresses was in the Salton Trough south of the epicenter (Figures 3, 4) thus adding weight to the idea that rupture directivity and dynamic stress amplitudes are important factors in determining the distribution of dynamic triggering (Gomberg et al. 2001, Hough and Kanamori 2002).

The Salton Trough is an extensional tectonic regime characterized by frequent earthquake swarms (Figure 3), geothermal areas, and Quaternary volcanism. The triggered response to the Hector Mine earthquake, which included three M>4 earthquakes, was centered beneath 1) the northern end of the Salton Trough in the vicinity of Indio ($\Delta \sim 87$ km), 2) the south end of the Salton Sea in the vicinity of the Obsidian Buttes volcanic field ($\Delta \sim 165$ km), and 3) in the Mexicali Valley in the vicinity of the Cerro Prieto geothermal field in Baja California at $\Delta \sim 260$ km (Hough and Kanamori 2002, Glowacka et al. 2002). Three sites northwest of the epicenter showed a weaker triggered response: the Coso volcanic field at $\Delta \sim 250$ km (Prejean et al. 2004), the north flank of Mammoth Mountain at the west margin of Long Valley caldera at $\Delta \sim 450$ km (Johnston et al. 2004a), and the Geysers geothermal field at $\Delta \sim 750$ km (Gomberg et al. 2001).

With the exception of Mammoth Mountain and Cerro Prieto, the onset of the triggered seismicity coincided with arrival of the surface waves from the Hector Mine earthquake. The onset of seismicity with respect to surface wave arrivals was apparently delayed by $\Delta t \sim 20$ minutes at Mammoth Mountain and $\Delta t \sim 2$ hours at Cerro Prieto. Notably, the triggered response at both Mammoth Mountain and Cerro Prieto included deformation transients detected by borehole dilatometers and tiltmeters, respectively (Johnston et al. 2004a, Glowacka et al. 2002).

8.02.2.3 The M_w 7.9 Denali Fault earthquake of 3 November 2002

The M=7.9 Denali Fault earthquake of 3 November 2002 produced the most widely recorded remote dynamic triggering through mid-2006. The earthquake, which was centered 65 km east of Denali National Park, Alaska, resulted from a complex rupture with maximum surface displacements reaching 8.8 meters (Eberhart-Phillips et al. 2003, Rowe et al. 2004).With a seismic moment ($M_0 \sim 4 \times 10^{20}$ N-m) comparable to that of the 1906 San Francisco earthquake, it was the largest earthquake to strike North America since the Mw=9.2 Anchorage megathrust earthquake of 27 March1964 (Plafker 1969). The unilateral rupture produced pronounced directivity with peak amplification of dynamic stresses directed to the southeast through British Columbia and the western United States. With the exception of the Katmai volcanic cluster 740 km southwest of the epicenter, all recognized sites of dynamic triggering were located southeast of the epicenter in the sector of maximum directivity that spanned the areas responding to the Landers and Hector Mines earthquakes (Figure 4). In all cases, the onset of dynamic triggering developed as a seismicity rate increase during passage of the Denali Love and Rayleigh waves. In three cases, Mount Rainer, Long Valley caldera, and Yellowstone, delayed earthquake swarms followed the initial surge in triggered seismicity by $\Delta t \sim 2.5$ hrs, 23.5 hrs, and 8 days, respectively (Prejean et al. 2004, Husen et al. 2004b).

The Yellowstone volcanic system and the central Utah seismic zone, where peak dynamic stresses ranged from ~0.2 to 0.3 MPa, provided the most energetic recorded triggered response to the Denali earthquake (Husen et al. 2004b, Pankow et al. 2004). In these locations, the seismicity rate increases were clearly evident in earthquake catalogs with compelling β-statistics on the order of ~10 to 30. Yellowstone responded with pronounced changes in the hydrothermal system in addition to the widespread seismicity increase (Husen et al. 2004a). The former included eruption pattern changes in 12 out of 22 instrumented geysers as well as transient temperature changes and boiling in a number of hot springs. Notably, geysers that responded to previous nearby (distances < 200 km) M~7 earthquakes did not respond to the Denali earthquake (Husen et al. 2004b). Seismicity increased over much of the Park with some 250 located earthquakes detected within the first 24 hours after the Denali earthquake, and it remained elevated over the next 30 days. Bursts of triggered seismicity within Yellowstone caldera tended to be concentrated in the vicinity of major geothermal areas.

Seismic activity increased at a number of sites along the Intermountain Seismic Belt (ISB) through central Utah following passage of the Denali surface waves (Pankow et al. 2004). Tectonically, the Utah section of the ISB is characterized by east-west extension accommodated normal to oblique slip along northerly striking faults. The clusters of triggered seismicity through central Utah showed no obvious correlation with the Quaternary volcanic vents common in the southern part of the area. The many hot springs along the ISB appear to be associated with deep fault-zone circulation rather than mid-crustal magmatic sources. High-resolution hypocentral locations showed that the triggered clusters tended to be spatially separated from background seismicity. The triggered activity, which included a M=3.2 earthquake, decayed to background levels over about 25 days. A site of triggered seismicity near Cedar City in southwestern Utah also responded with triggered seismicity following the 1992 Landers earthquake.

The remaining instances of dynamic triggering by the Denali Fault earthquake were not evident in regional earthquake catalogs but were uncovered by examining high-pass filtered seismograms from broad-band and strong motion instruments from individual seismic stations within these networks. The results revealed six sites in southern British Columbia (Gomberg et al. 2004), two sites in western Idaho (Husker and Brodsky 2004), five sites along the west coast states including Mount Rainer in Washington, the Geysers geothermal field in northern California, Mammoth Mountain-Long Valley caldera in eastern California, and the Coso volcanic field in southern California (Prejean et al. 2004). Two earthquakes with magnitudes M=1.8 and 2.5 located ~125 km offshore in the southern California borderland (4,003 km from the Denali epicenter) that occurred during passage of the Denali surface wave coda and may also represent triggered activity, although the statistical significance of such isolated events is difficult to establish (Prejean et al. 2004).

The sole instance of dynamic triggering orthogonal to the sector of rupture directivity involved a burst of small ($M \leq 2.0$) earthquakes in the Katmai volcanic cluster 740 km southwest of the Denali epicenter that began during the surface wave train and died out over the next several hours (Moran et al. 2004). Indeed, it appears that seismicity rates

may have temporarily slowed at Mt. Wrangell and Mt. Veniaminof volcanoes following the Denali earthquake at distances of 247 km and 1,400 km southwest of the epicenter, respectively (Sanchez and McNutt 2004). The Katmai volcanic field appears to be particularly susceptible to dynamic triggering in that it has responded to four previous earthquakes in the M = 6.8 to 7.0 range that were located at distances between 60 and 160 km (Moran et al. 2004, Power et al. 2001).

8.02.3 The Search for Additional Evidence for Dynamic Triggering

The compelling evidence for dynamic triggering provided by the 1992 Landers earthquake spawned a search through both historic and instrumental records for evidence of dynamic triggering from previous earthquakes as well as for new instances of dynamic triggering associated with new large earthquakes (Table 1). As the evidence accumulates, it's becoming clear that dynamic triggering at remote distances is a relatively common phenomenon.

<Table 1 near here>

8.02.3.1 Anecdotal evidence for pre-instrumental dynamic triggering

In an extensive search through archive newspapers and correspondence for felt reports, Hough (2001) and Hough et al.(2003) find evidence for dynamic triggering at distances up to1,000 km or more by two of the four $M_W > 7$ New Madrid, Missouri earthquakes of 1811-1812 and the $M_W > 7$ Charleston, South Carolina, earthquake of 1886. These results are particularly intriguing because they offer evidence for dynamic triggering in a low-seismicity-rate, low-strain rate intraplate environment characterized by a transpressional stress regime (see Reinecker et al. 2004).

Steeples and Steeples (1996) and Meltzner and Wald (2003) investigated the distribution of aftershocks and possible triggered earthquakes for the great ($M_W \sim 7.8$) San Francisco earthquake of 1906. They found evidence for 9 earthquakes in the magnitude range M ~4 to ~6 within the first 48 hours after the 1906 mainshock. The most distant, a M~4 earthquake in western Arizona at Δ ~900 km, occurred during the seismic waves from the 1906 mainshock and is a likely candidate for dynamic triggering. Earthquakes marginally beyond the aftershock zone and thus potential candidates for remote dynamic triggering include a M~6.1 event near the south end of the Salton Sea (Δ ~700 km, $\Delta\tau$ ~ 11.3 hrs) and M~3.5 and M~4.5 earthquakes in western Nevada at Δ ~400 and 410 km and $\Delta\tau$ ~ 32.8 and 39.0 hrs, respectively.

8.02.3.2 Instrumental evidence from around the globe

Reviewing instrumental records from the dense seismic network around the Geysers geothermal field in the northern California Coast Ranges between 1988 and 1994, Stark and Davis (1995) and Gomberg and Davis (1996) found instances of abrupt, temporary increase in the rate of small earthquakes (M<3) to dynamic stresses from eight regional earthquakes with magnitudes between M=6.6 – 7.7 at distances between Δ =212 – 2,500

km. The Geysers geothermal field, which seems particularly susceptible to dynamic triggering, subsequently responded to the 1999 Hector Mine earthquake (Gomberg et al. 2001) and the 2002 Denali Fault earthquake located 3,120 km to the northwest (Prejean et al. 2004).

Just over two months before the Landers earthquake, a $M_W = 5.4$ earthquake on 13 April 1992 occurred within the Roer Valley Graben near Roermond, The Netherlands (Camelbeeck et al. 1994). A series of earthquakes 40 km to the southeast (along strike with the northwest striking normal faults forming the graben) began some three hours after the mainshock. Camelbeek et al. (1994) suggest that these represent remotely triggered earthquakes.

Brodsky et al. (2000) document an increase in $M \geq 2$ seismicity over much of continental Greece abruptly as the surface waves from the M=7.4 Izmit, Turkey, earthquake of 17 August 1999, swept through the region at distances from $\Delta \sim 400$ to $\sim 1{,}000$ km. The largest of the triggered earthquakes exceeded the catalog completeness threshold $M > 3.5$, and these larger events tended to be located away from areas characterized by high background seismicity. Greece is dominated by pervasive normal faulting with widely distributed hot springs, which derive their heat from deep crustal circulation along the normal faults rather than mid-crustal magma bodies (Brodsky et al. 2000). Greece has no history of volcanism.

Mohamad et al. (2000) describe evidence for remotely triggered seismicity in a localized cluster along the Syrian-Lebanese border from the dynamic stresses generated by the $M_S = 7.3$ Gulf of Aqaba earthquake of 22 November 1995 that resulted from strike-slip rupture along a segment of the sinistral Dead Sea Fault some 500 km to the south. The triggered seismicity began 2.8 hours after the mainshock and produced over 20 small earthquakes over the next 3.5 hours, the largest of which was a $M = 3.7$ event. The triggered cluster occurred near a restraining bend in the sinistral Yammouneh fault some 50 km north of the volcanic and geothermal area in the Golan Heights.

The epicenters of $M_w = 6.5$ and 6.4 earthquakes in the South Iceland Seismic Zone on 17 and 21 June 2000, respectively, were separated by just 17 km in an east-west direction. Both earthquakes involved dextral slip on north-striking planes. As described by Arnadottir et al. (2004), the first and largest of these earthquakes triggered widespread seismicity on the Reykjanes Peninsula to distances of ~100 km to the west as well as significant slip on at least three faults in the Reykjanes Peninsula while the second slightly smaller earthquake, although 17 km further west, did not. The triggered seismicity included three M~5 earthquakes that followed the M=6.5 event by seconds to minutes. Arnadottir et al. (2004) conclude that these M~5 earthquakes were beyond the range for Coulomb failure due to static stress changes from the M=6.5 mainshock and thus that they were likely triggered by dynamic stresses. Their analysis of continuous GPS geodetic data spanning the Reykjanes Peninsula indicates that the geodetic moment for the second of the triggered M~5 earthquakes ($\Delta \sim 78$ km) was an order of magnitude larger than its seismic moment and that the large Coulomb stress change from this largely aseismic, slow earthquake was sufficient to trigger the third and most distant M~5 event

some four minutes later through quasi-static stress transfer. This, then, provides a possible example of earthquake triggering as a secondary response to a locally triggered deformation transient consistent with the slow fault slip model proposed by Anderson et al. (1994).

Singh et al. (1998) examined Mexican seismograms and earthquake catalogs spanning the interval 1920 through 1957 for evidence of dynamic triggering in the Valley of Mexico within the Trans Mexican Volcanic Belt from large (M 7.6 to 8.0) subduction zone earthquakes along the southwest coast of Mexico. They identified "abrupt" (within two days) seismicity increases following seven out of thirteen subduction zone earthquakes at distances of $\Delta \sim 303$ to ~588 km. In three cases, they identified seismicity increases after a delay of some 30 days following the subduction zone earthquake. Three of the subduction zone earthquakes produced no recognizable seismicity rate increases. The latter included a M=8.0 earthquake at a distance of $\Delta \sim 405$ km and a M=7.7 earthquake at $\Delta \sim 347$ km. The three delayed responses of $\Delta t \geq 30$ days certainly raise some interesting questions regarding statistical significance and a causal link between dynamic stresses and triggered seismicity.

In a study of possible dynamic triggering in the Taiwan region, Wen et al. (1996) examined the catalog for the Taiwan Telemetered Seismic Network (TTSN) from 1973 through 1994 for evidence of seismicity increases following 12 regional earthquakes with magnitudes from M = 6.5 to 7.1 at distances of $\Delta \sim 138$ to 2,959 km. In nine cases they found a four-fold increase in the number of $M \geq 4.5$ earthquakes in the 15-day period following a $M \geq 6.5$ earthquake with respect to the 15 preceding days and in 10 cases a seven-fold increase in $M_L \geq 4.0$ earthquakes. The significance of this result remains a question. Taiwan is dominated by a compressional-transpressional stress regime (Reinecker et al. 2004) although, locally, the northern end of the island, which includes the Quaternary Tatun volcanic group and associated geothermal activity, is an extensional regime (Song et al. 2000). Wen et al. (1996) do not address the spatial distribution of the triggered seismicity.

Somewhat surprisingly, evidence in the published literature for dynamic triggering in Japan is sparse (Harrington and Brodsky 2006). Japan is well monitored by dense seismic and deformation networks, and it is populated by many active volcanoes and geothermal systems. Harrington and Brodsky (2006) suggest this insensitivity to triggering may result from compressional tectonics that dominates the country or perhaps the high occurrence rates of large mainshocks that serve to frequently disrupt blockages in fracture systems thereby preventing a buildup of differential pore pressures between hydrologic units that might otherwise respond to dynamic stresses. Exceptions appear to be limited to volcanic systems on Kyushu in southern Japan, which is a area of extensional tectonics. Miyazawa et al. (2005) describe evidence for multiple increases in isolated tremor and microearthquakes at Aso volcano in central Kyushu, Japan, following large, distant earthquakes including the M_W=7.7 Chi-Chi, Taiwan earthquake of 20 September 1999. Harrington and Brodsky (2006) show evidence for increased seismicity on Kyushu following the 26 December 2004 M_W=9.0 Sumatra earthquake. Two particularly intriguing contributions from Japan describe evidence for dynamic triggering of deep,

low-frequency earthquakes along the Nankai subduction zone beneath Honshu and bursts of shallow microearthquakes on Iwo Jima in the Volcano Islands group situated between the Marianas and Izu island arcs some 1,250 km south of Tokyo.

The island of Iwo Jima represents the resurgent dome of a large submarine caldera. (Iwo Jima, or Sulfur Island, is best known as the site of a major World War II battle.) It has a well developed geothermal system and has produced a Holocene volcanic eruption and several recent phreatic explosions. Ukawa et al. (2002) examined Iwo Jima seismograms for 21 M>7 earthquakes located within 3,000 km of the island and found four instances when local seismicity increased during passage of the surface waves from the distant earthquakes. In each case, the triggered response was characterized by an abrupt increase in local microearthquake activity that died out over the next 6 to 15 minutes. Iwo Jima seismograms showed a similar triggered response to the surface waves from the great M=9.1 Sumatra-Andaman Islands earthquake of 26 December 2004 (Ukawa, personal communication 2005).

The evidence for dynamic triggering of deep low-frequency tremor beneath Japan is notable in that it, together with the Tonga example described in the next paragraph, are the only documented instances of dynamic triggering not confined to the upper, brittle crust. Deep low-frequency (DLF) tremor is associated with subduction of the Philippine Sea plate beneath southwestern Japan (Obara 2002). This non-volcanic tremor consists of clusters of low-frequency (1-10 Hz) earthquakes near the base of the crust at depths from 20 to 30 km and appears to be associated with the upward flow of hydrous fluids liberated by dehydration of the subducting slab. Obara (2002) suggests that fluctuations in the DLF activity in the spring of 2001 may have been modulated by local M~6 earthquakes at distance of 40 to 50 km. Miyazawa and Mori (2005) applied a β-statistic analysis to the DLF activity and found convincing evidence of a rate increase as the surface waves from the M_w = 8.1 Tokachi-oki earthquake of 25 September 2003, some 1,000 km to the northwest, propagated through the area. They found a similar response to the surface waves from a M_w = 7.3 earthquake in Siberia 40 hours later (27 September) located ~4,000 km to the west. Subsequently, Miyazawa and Mori (2006) document that the Rayleigh waves from the 2004 Sumatra-Andaman Islands earthquake modulated deep low-frequency tremor along a 500 km-long zone beneath southwestern Japan suggesting that dilatational stresses may be important in the triggering process.

A M_w = 7.6 earthquake on 19 August 2002 at a depth of ~665 km beneath the Tonga subduction zone was followed by M_b = 5.9 and M_w=7.7 earthquakes in the same depth range with delays of 2.2 and 7.4 minutes, respectively. As described by Tibi et al. (2003), the latter two earthquakes occurred in a previously aseismic volume located ~290 km southwest of the initial M_w = 7.6 event. They find that the static Coulomb stress change at this distance from the initial M_w = 7.6 earthquake is small and conclude that these earthquakes were most likely dynamically triggered by the body waves from the M_w = 7.6 earthquake. A similar sequence of deep triggering may be represented by a M_w = 7.1 earthquake in a previously aseismic volume that followed a M_w = 6.8 slab earthquake at a distance of 257 km by 25 minutes (Tibi et al. 2003).

8.02.3.3 Aftershocks and stress triggering at near to intermediate distances

Stress triggering at near and intermediate distances from a large earthquake is tied to the long-standing question of aftershock generation (Nur and Booker 1972, Gomberg et al. 2003, Kilb et al. 2002). The most intense aftershock activity generally occurs within a source dimension of the mainshock rupture (the near field) where static and dynamic stresses have comparable amplitudes and minimal temporal separation (Figure 1). Distal portions of an aftershock zone, however, commonly extend one to two source dimensions beyond the rupture zone in the range where static and dynamic stresses begin to assume separate identities. Efforts to distinguish between static and dynamic stress triggering in aftershock zones have sought evidence in spatial distribution of aftershocks with respect to stress shadows predicted by static stress transfer models (Felzer and Brodsky 2005, Kilb et al. 2002, also see Chapter 7) as well as for the influence of rupture directivity (Gomberg et al. 2003) and the variation in peak dynamic stress amplitudes with distance (Felzer and Brodsky 2006). Pollitz and Johnston (2006) point to the relative absence of aftershocks following slow earthquakes along the central section of the San Andreas Fault compared with typical earthquakes of similar location and seismic moment as evidence for the importance of dynamic stresses in aftershock production. Based on these studies, it seems clear that dynamic stresses are important in aftershock generation at all distances, particularly for short times (hours) following the mainshock.

Hough (2005) explores the dynamic triggering potential of moderate earthquakes ($M < 7$) in the transition between the distal aftershock zone and remote distances by stacking β-statistic maps for 15 moderate (M 5.3 to 7.1) earthquakes in central and southern California. She found evidence for slightly elevated seismicity levels in the 140- to 200-km distance range (> two source dimensions for $M < 6$ earthquakes) during the month following the respective mainshocks and suggests this may represent seismicity dynamically triggered by the large-amplitude S waves critically reflected from the base of the crust (SmS). Some of these elevated seismicity levels are located within the traspressive stress regimes adjacent to the San Andreas Fault system. Because the elevated β-statistics in these examples are modest ($\beta \sim 2$, see Appendix I), this intriguing result remains ripe for further testing.

This is currently a rapidly evolving research topic with the relative merits of static vs. dynamic aftershock triggering the subject of energetic exchanges between advocates of one or the other viewpoint (Voisin et al. 2004, Harris and Day 1993, Harris et al. 2002, Stein 1999). Accumulating evidence suggests that dynamic triggering does indeed have a role in aftershock generation as well as in complex rupture processes in which major earthquakes consists of multiple large sub-events (e.g. Aagaard et al. 2004, Rybicki et al. 1985, Antonioli et al. 2002, Voisin et al. 2000).

8.02.3.4 Triggering by solid Earth tides

One of the long-standing puzzles in seismology has been why the periodic stressing of the Earth's crust by solid Earth tides appears to have little or no influence on temporal patterns of earthquake occurrence – particularly given evidence that broad sections of the

crust are in a state of incipient failure. The generally acknowledged exceptions appeared to be limited to shallow earthquake swarm activity in volcanic and geothermal areas (Klein 1976, Tolstoy et al. 2002). Recently, however, Tanaka et al. (2004) and Cochran et al. (2004) present convincing evidence that the solid Earth tides in combination with ocean loading tides do indeed modulate the occurrence of crustal thrust earthquakes in convergent margins around the Pacific basin at the 10 to 20% level. The key appears to lie in correlating well-constrained focal mechanisms from a massive number of earthquakes (tens of thousands) with the phase of the tidal cycle that augments the local tectonic stress directions. These results are consistent with inferences based on laboratory measurements that cyclical stressing at the 0.001 to 0.004 MPa level should modulate the occurrence of background seismicity (Beeler and Lockner 2003, Lockner and Beeler 1999). The evidence for tidal triggering on reverse faults in Japan (Tanaka et al. 2004) presents an intriguing contrast to the apparent insensitivity of the many volcanic and geothermal centers in Japan to remote dynamic triggering by large earthquakes (Harrington and Brodsky 2006). While strictly speaking solid Earth tides represent a quasi-static process (the inertial component in the equations of motion are negligible for solid Earth tides), they suggest a lower bound for amplitudes (~0.001 MPa or ~0.01 bar) that low-frequency dynamic stresses must reach to have the potential for dynamic triggering.

8.03 TRIGGERED RESPONSE CHARACTERISTICS

Unraveling the physics behind dynamic triggering requires identifying key characteristics of the triggered response and their variations from site to site for a given earthquake as well as their variations at a given site for different source earthquakes. In this section, we highlight some of the more obvious of these characteristics based on published descriptions of dynamically triggered seismicity.

8.03.1 Tectonic Setting

The tectonic setting and stress regime have a first-order effect on the style of earthquake activity in any given area. Accumulating evidence indicates that these environmental factors also have an influence on patterns of remotely triggered seismicity.

8.03.1.1 Crustal triggering

Most well-documented, instrumentally recorded instances of dynamic triggering within the brittle, seismogenic crust (depth less than15 to 20 km) are associated with extensional or trans-tensional tectonic regimes. In many of these cases, the triggering coincides with areas of elevated background seismicity and commonly (but not exclusively) with geothermal areas and areas of Quaternary to Recent volcanism.

Extensional and transtensional stress regimes have two closely related properties that might enhance their susceptibility to dynamic triggering. First, the least principal stress has a sub-horizontal orientation. Because extension cracks tend to form in planes normal to the least principal stress, extensional stress regimes facilitate the upward migration of

crustal fluids from warmer, higher-pressure pressure conditions at depth toward the surface through vertically oriented cracks. One consequence of this property is the propensity for geothermal areas (and volcanism) to be concentrated in extensional regimes. Second, as illustrated in Figure 5A, faults in an extensional regime are intrinsically weaker than those in compressional regimes given a uniform coefficient of friction and Andersonian faulting (Sibson 1982). Hough and Kanamori (2002), for example, suggest that elevated pore pressures and temperatures associated with geothermal areas should enhance this difference (illustrated by the dashed Mohr's circle in Figure 5A).

<Figure 5 near here>

There are, however, exceptions to this pattern. One involves the evidence for remote triggering based on pre-instrumental descriptions of felt shaking in the transpressional regimes of Ohio River Valley area and Atlantic coast states following the 1811-1812 New Madrid, Missouri, earthquakes and the Charleston, South Carolina earthquake of 1887 (Hough 2001, Hough et al. 2003). Another involves Hough's (2005) evidence for apparent seismicity increases at distances of 70-200 km triggered by dynamic stresses associated with super-critical SmS waves from 15 moderate earthquakes (M ~5) in coastal California. In this case, several areas of slightly elevated β-statistic were located within the transpressional Coast Ranges. Hough et al. (2005) also suggest that SmS waves may have triggered a M>7 earthquake a few minutes after the $M_W = 7.8$ earthquake of 1905 in the compressional Kangra region of India. We have yet, however, to see evidence for remote dynamic triggering in well instrumented compressional or stable intraplate regimes on a scale comparable to that observed in tectonically active extensional or transtensional regimes.

Subduction-related volcanic centers are located on convergent plate boundaries. Locally, however, they commonly coincide with a zone of crustal extension and transtensional deformation associated with upward flexure of the overriding plate. This is the case for the Katmai volcanic field in Alaska (Moran 2003), for example, as well as most of the Cascade volcanoes in the Pacific Northwest states. Mt. Rainer volcano in Washington State is exceptional with its setting in a transpressional stress regime. Even here, however, focal mechanisms for earthquakes occurring within the edifice of the volcano or shallow crust immediately below the volcano show dominantly normal faulting (Moran et al. 2000).

This raises a question regarding the meaning of the crust being in a state of incipient failure nearly everywhere (Zoback and Zoback 2002). Within the context of Figure 5A, a weak, extensional crust offers no particular advantage over a strong compressional crust if incipient failure means that, on average, the stress level everywhere hovers below the failure strength by some common increment, $\Delta\tau$. (this corresponds to a stress-state defined by a line parallel with but incrementally below the Coulomb failure curve, $CFF = 0$ in Figure 5A) A weak crust would be more susceptible to dynamic triggering, however, if average stress levels were some large fraction of the failure stress (represented by a line with a smaller slope than that for $CFF = 0$ in Figure 5A). Currently available data seem ambiguous on this point. Any diminished propensity for triggering in stable intraplate

regions due to a stronger crust may be at least partially offset, however, by the fact that seismic wave amplitudes generally decay more rapidly with distance in tectonically active regimes than in stable intraplate regions because of higher intrinsic attenuation and the presence of velocity inversions in the lower crust and upper mantle that partially channel both body wave and normal mode (surface wave) energy within depth intervals below the brittle crust (Bakun and McGarr 2002).

8.03.1.2 Sub-crustal triggering

The few documented instances of subcrustal dynamic triggering are tied to seismogenic subducting slabs beneath Japan and the Tonga-Fiji arc. Remotely triggered increases in low-frequency (DLP), tremor-like seismicity at depths of 30 to 40 km beneath western Honshu and Shikoku appear to be related to dehydration of the Philippine Sea plate as it slides beneath Japan along the Nankai subduction zone (Miyazawa and Mori 2005). Magnitude M ~ 7 earthquakes at depths of 500 – 600 km within the seismogenic subducting slab beneath the Tonga-Fiji arc have apparently triggered large ($M \geq 5.9$) earthquakes at comparable depths but at offset distances of ~300 km (Tibi et al. 2003). Green (2003) speculates that dynamic stresses likely triggered a phase change in metastable olivine within the slab resulting in relatively weak inclusions that deform in the ambient stress field leading to adiabatic shear heating and an earthquake.

8.03.2 Mainshock Source Mechanisms and Directivity

Both the most common and most compelling displays of remote dynamic triggering are associated with M>6.5 earthquakes on strike slip faults with unilateral rupture and pronounced directivity as exemplified by the Landers and Denali Fault earthquakes (and to a lesser extend by the Hector Mine earthquake). Large subduction zone earthquakes, however, also produce remote dynamic triggering as, for example, in the case of the Valley of Mexico (Singh et al. 1998), the subcrustal seismicity beneath Japan and the Tonga-Fiji arc (Miyazawa and Mori 2005, Tibi et al. 2003), and most recently, Iwo Jima (Ukawa et al. 2002) and Mt. Wrangell, Alaska (West et al. 2005)from the great (M_w=9.1) Sumatra-Andaman earthquake (Lay et al. 2005). In the latter, the sparse seismic coverage in the area of peak directivity may account for the fact that only two reports of remote triggering have yet to emerge following the largest earthquake in 40 years. The lack of published descriptions of remote dynamic triggering attributable to large normal fault earthquakes may be largely a matter of sampling. Few M>6.5 normal earthquakes have occurred in well-instrumented continental environments in the last 25 years.

8.03.3 Triggered Onsets and Delay Times

In most cases the onset of dynamically triggered seismicity at a given site begins not with the first arriving P wave from a distant mainshock but during or some time, Δt, after the arrival of the large-amplitude Love or Rayleigh waves. This observation suggests that, 1) the reference time, t_0, for dynamic triggering at remote distances should generally be taken to coincide with the local Love wave arrival time, and 2) that dynamic stresses with periods much below 20 to 30 seconds are not efficient at inducing widespread remote

triggering. Coincidence of a small, isolated earthquake in Long Valley caldera with the S-wave arrival from the Denali Fault earthquake (Prejean et al. 2004) may represent a rare exception surface wave triggering at remote distances. Clearly, this does not apply to dynamic triggering in the aftershock zone at near to intermediate distances where long-period surface waves have yet to emerge as a separate phase. Hough's (2005) inference from stacked β-statistic maps that SmS waves with frequencies in the 1 Hz range may induce dynamic triggering at intermediate distances, for example, stands as a possible example of short-period body wave triggering.

Reported delay times, Δt, between arrival of the dynamic waves, t_0, and the apparent onset of locally triggered seismicity vary from seconds ($\Delta t \sim 0$) to weeks or more. Delay times for the well-recorded instances of dynamic triggering from the Landers, Hector Mine, and Denali Fault earthquakes ranged from a few seconds to between 24-33 hours. Delay times reported for suspected dynamic triggering in the Taiwan region approach 15 days (Beresnev and Wen 1995, Wen et al. 1996) and, in the Valley of Mexico, ~30 days (Singh et al. 1998). The longer the delay time, of course, the more tenuous the case for a causal link between the dynamic stresses and a local seismicity rate increase. Statistically, instances of suspected triggering may be considered "instantaneous" if the first event in the sequence has a delay time $\Delta t < 3/\lambda$, where λ is the mean rate of the first n events in the sequence (see Appendix I). In this sense, triggered seismicity mimics an aftershock sequence to dynamic stressing (Brodsky, 2006). Establishing the significance of longer delay times ($\Delta t > 3/\lambda$) ultimately will depend on the credibility of a well-tested physical model that accounts for the delay between arrival of dynamic stresses and the local onset of brittle failure (section 8.04.2).

<Figure 6 near here>

It is important to bear in mind that reported delay times based on recording from standard, short-period seismic networks may overestimate actual delay times. In particular, evidence for short delay times is not likely to appear in standard earthquake catalogs because local earthquakes are typically masked by the large-amplitude surface waves from large earthquakes. The development of broad-band, high dynamic-range instrumentation and digital processing has greatly enhanced our ability to recognize the early onset of local earthquake activity within coda waves from large, distant earthquakes through effective filtering. Prejean et al.(2004), for example, found this to be the case in their search for dynamic triggering along the west coast of the United States following the M=7.9 Denali Fault earthquake of 2002 (Figure 6). Applying a β-statistic test to the Pacific Northwest and California earthquake catalogs produced no clear evidence for dynamic triggering. By applying a high-pass filter to seismograms from broad-band and strong motion instruments, however, they discovered a plethora of small earthquakes embedded in the strong surface waves from the Denali earthquake at four sites in Washington and California from Mount Ranier ($\Delta \sim 3{,}108$ km) south to the Coso volcanic field in southern California ($\Delta \sim 3{,}660$ km). (Figure 6 illustrates the value of spectrograms in identifying small, local earthquakes in the surface wave coda from large earthquakes.) Small delay times were the rule for most instances of dynamic triggering from the Denali Fault earthquake.

This underscores two points: 1) dynamic triggering with small delay times ($\Delta\tau \sim 0$) with respect to peak dynamic stresses is probably considerably more common than generally realized, and 2) our ability to detect dynamic triggering remains extremely uneven depending critically on the distribution of dense, high-quality seismic networks that include broad-band, high-dynamic range digital instruments.

8.03.4 Repeat Triggering and Recharge Times

Several sites with documented remote triggering have responded more than once to the dynamic waves from distant earthquakes (see Table 2). The most notable example is the Geysers geothermal field in northern California, which has responded to at least eleven different earthquakes. Other repeating sites include the Coso geothermal field in southeastern California, the Katmai volcanic field, Alaska, and in Japan, Iwo Jima, Aso volcano, and the Nankai trough subduction zone. Each responded to at least four different earthquakes. In each of these cases, the response was much the same from one earthquake to the next with the triggered seismicity beginning during the surface wave train and persisting for at most an hour or so. With the exception of the deep, long-period earthquakes along the Nankai trough (Miyazawa and Mori, 2006), the triggered seismicity appeared as a rapid-fire series of overlapping brittle-failure earthquakes (spasmodic bursts) and involved much of the seismogenic volume of the respective systems.

<Table 2 near here>

A number of other sites listed with multiple responses in Table 2 do not strictly involve repetitive sequences. Long Valley caldera, for example, is commonly referenced as a site that has responded to at least three distant earthquakes. Each instance, however, has involved spatially distinct crustal volumes within this large, distributed volcanic field. The Landers response was the most energetic involving the entire seismogenic section of south moat of the caldera (Hill et al. 1995) while response to the Hector Mine and Denali Fault earthquakes involved limited, non-overlapping volumes beneath the north and south side of Mammoth Mountain, respectively (Johnston et al. 2004a). The delayed response ($\Delta t \sim$ 24 hours) to the Denali Fault earthquake in the south moat of Long Valley caldera was limited to a relatively shallow volume that had not been previously active (Prejean et al. 2004). Even when the same crustal volume appears to show repetitive triggered responses, successive responses may involve different fault sets with differing orientations.

Identification of strictly repeating sites raises the question of recharge times. Each instance of remotely triggered seismicity releases locally stored energy, thus moving the responding site incrementally away from the near-critical state that existed just prior to arrival of the dynamic stresses. The time required for the site to return to a near-critical state (the recharge time) will depend on a host of factors including 1) the energy released during the most recent episode of seismic activity whether remotely triggered or not, and 2) the background rate of active processes feeding energy into the local crustal volume

(Herrington and Brodsky 2006, Miyazawa et al. 2005). As an example of (1), Rabaul caldera (Papua New Guinea) responded to a M7 earthquake at a distance of 180 km with a pronounced earthquake swarm but produced no detectable activity in response to a second M7 earthquake two month later at a distance of only 60 km (Mori et al. 1989). Recharge times for the Geysers geothermal area appear to be short -- a matter of months or less (Gomberg and Davis 1996). They are apparently much longer (but ill-constrained) for Long Valley caldera where none of the triggered sites are strictly repetitive. Recharge times and their spatial-temporal fluctuations complicate efforts to establish triggering thresholds for dynamic stresses (e.g. Gomberg 1996, Gomberg and Johnson 2005). At the same time, they offer important clues to the processes behind dynamic triggering at any given site.

8.03.5 Peak Dynamic Stresses, Triggered Magnitudes and Durations,

Seismic wave amplitudes responsible for dynamic triggering are variously reported as peak dynamic stress, T_p, or peak dynamic strain, ε_p. In the plane-wave approximation, peak dynamic strain is proportional to peak particle velocity, $\mathring{u}$ divided by the phase velocity, or $\varepsilon_p \sim \mathring{u}\, v_s^{-1}$ for shear waves, and $T_p \sim G(\mathring{u}\, v_s^{-1})$ where G is the shear modulus (commonly taken as $G \sim 3\text{x}10^4$ MPa) and v_s is the shear wave velocity (e.g. see note 20 in Hill et al. 1993). Although peak dynamic stresses at depth will in general differ from those based on seismograms recorded on the Earth's surface, they can be estimated given a reasonable model for the physical properties of the underlying crust (Gomberg, 1996). In computations of stress amplitudes at depth, for example, the tendency for surface wave displacement amplitudes and strains to decrease with depth will be offset to one degree or another by the tendency of elastic moduli to increase with depth.

Reported peak dynamic stresses associated with remotely triggered seismicity range from 0.01 MPa ($\varepsilon_p \sim 0.3$ microstrain) at the Coso volcanic field 3,660 km from the $M_W = 7.9$ Denali Fault earthquake (Prejean et al. 2004) to ~1 MPa ($\varepsilon_p \sim 3$ microstrain) or more for the Little Skull Mountain earthquake 240 km north of the M=7.4 Landers earthquake (Hill et al. 1993, Anderson et al. 1994). Peak dynamic stresses can easily exceed 4 MPa within the transitional region to the aftershock zone and near field of a large earthquake (Kilb et al. 2002). The large range in peak dynamic stresses (or strains) that have resulted in remote triggering together with variations in intrinsic site characteristics and recharge times indicate that the triggering process does not depend on a simple minimum amplitude threshold for dynamic stresses to be effective. Thus, although most instances of dynamic triggering involve dynamic strains, $\varepsilon_p \geq 1\text{x}10^{-6}$, or dynamic stresses, $T_p \geq 0.03$ MPa (Gomberg and Johnson 2005), this is neither a necessary nor sufficient threshold for dynamic triggering (most areas with $T_p \geq 0.03$ MPa are not triggered and some areas with $T_p < 0.01$ MPa are triggered). The weight of evidence at this point suggests that for a given peak amplitude, dynamic stresses in the periods range 20 to 30 seconds are more effective at inducing a triggered response than those at higher frequencies and that a lower bound on the peak dynamic stress capable of inducing a triggered response may be at the level of tidal stresses, or ~0.001 MPa at periods of 12 to 24 hours (Beeler and Lockner 2003; also see section 8.02.3.4).

Durations of dynamically triggered seismicity sequences range from a few minutes to several weeks. Short-lived episodes of triggered seismicity often appear as a rapid-fire sequence of over-lapping, brittle-failure earthquakes (spasmodic bursts) within the surface wave train. Longer-lived episodes more commonly evolve as earthquake swarms or foreshock-aftershock sequences with a temporal decay well described by a modified Omori law of the form

$$n(t) = k / (t + c)^p \qquad (3$$

where $n(t)$ is the number of earthquakes per unit time t, and k, c, and p are parameters (Kisslinger and Jones 1991). Pankow et al. (2004), for example, use this relation to estimate durations of ~25 days for the seismicity triggered in central Utah by the 2002 Denali Fault earthquake. Hainzl and Ogata (2005) describe a promising application of the epidemic type aftershock sequence (ETAS) model that can be used to recognize the modulating role pore-pressure diffusion in swarm-like triggered sequences. Generally speaking, longer durations tend to be associated with more energetic episodes of triggered seismicity. Indeed, Brodsky (2006) argues that the duration of most triggered sequences can in principle be predicted from the cumulative seismic moment of events triggered during the passage of (dynamic stressing). The validity of this conjecture will be tested with recordings of future instances of remote triggering on broad-band, high-dynamic range instrumentation such that triggered events within the coda of large-amplitude dynamic waves can be clearly resolved.

8.03.6 Dynamically Triggered Deformation

Only three sites that have responded to dynamic stresses with remotely triggered seismicity are equipped with continuous, high-resolution deformation monitoring instrumentation: Long Valley caldera, California, the Reykjanes Peninsula, Iceland, and the Cerro Prieto geothermal field, Mexico. At each of these sites, the triggered seismicity was accompanied by a deformation transient an order of magnitude larger than can be attributed to the summed slip of the triggered earthquakes.

Deformation transients in Long Valley caldera triggered by the 1992 Landers earthquake were recorded by a borehole strainmeter (dilatometer) and a long-base tiltmeter. The deformation transients beneath Mammoth Mountain triggered by the 1999 Hector Mine and the 2003 Denali Fault earthquakes were both recorded by three borehole strainmeters. In each case, the deformation transient began during the surface wave train. As illustrated in Figure 7, the Landers deformation transient grew to a peak amplitude of ~0.3 microstrain over a period of five days in parallel with the cumulative seismicity (Hill et al. 1995, Johnston et al. 1995) while the Hector Mine and Denali Fault transients more closely resembled strain steps reaching peak amplitudes of ~0.1 microstrain over a period of roughly 10 minutes (Johnston et al. 2004b).

<Figure 7 near here>

The deformation transient across the Reykjanes Peninsula triggered by the 17 June 2000 M=6.5 earthquake was captured by a pair of continuous GPS stations located on either side of the Peninsula. Displacements of campaign-mode GPS stations occupied in July 2000 with respect to a 1998 survey indicate that most of the coseismic deformation can be attributed to aseismic slip (a slow earthquake with a geodetic moment of ~$7x10^{17}$ Nm) on a fault 78 km (approximately four source dimensions) west of the M=6.5 mainshock (Arnadottir et al. 2004).

Ground deformation in the Mexicali Valley area, Mexico, a pull-apart basin formed by the right-stepping offset between the dextral Cerro Prieto fault zone and the southern end of the dextral Imperial fault, is monitored by both crack meters (creep meters) and tiltmeters. The crack meters recorded subsidence of ~10 cm along the southern end of the Imperial fault accompanied by the onset of local microearthquake (M<2.5) activity that developed as the surface waves from the 1999 Hector Mine earthquake 260 km to the north passed through the area. Some 30 hours later, tiltmeters recorded the onset of pronounced deformation within the Cerro Prieto geothermal area within the Mexicali Valley followed by the onset in a surge in M>2.5 seismicity beneath the geothermal field that gradually slowed following a M=4.1 earthquake beneath the geothermal field a day later (Glowacka et al. 2002).

8.04 PROPOSED MODELS

The convincing display of dynamic triggering by the1992 Landers earthquake spawned a host of physical models to explain how relatively low amplitude oscillatory seismic waves can trigger earthquakes at distances of 100s to 1,000's of km. Here we describe the more widely cited of these models and the conditions and locations under which each is viable.

8.04.1 Triggering by Frictional Failure

This class of models involves direct triggering with the dynamic stresses providing the stress increment necessary to exceed the frictional strength of faults, thus leading to unstable slip and local earthquakes. Frictional models are commonly discussed within the context of a steady loading rate (far-field plate motion or the steady extension of a spring in the case of a slider block model) and a "clock change". A "clock advance", for example, results if a small dynamic perturbation in the applied stress triggers a slip event that would not have otherwise occurred until the failure threshold was reached under the steady, far-field loading rate (e.g. Gomberg et al. 2005, Gomberg et al. 1997, Perfettini et al. 2003). One consequence of a clock advance in this context is that the time to the next slip event under far-field loading is inversely proportional to the far-field loading rate. Frictional models involve fluids only indirectly through the effect of pore pressure on the effective normal stress (or equivalently, an effective coefficient of friction) on fault planes. For dynamic stresses with periods of minutes or less, the rock matrix will behave as an undrained poro-elastic medium with fluid transport having a negligible influence on pore pressure fluctuations (Cocco and Rice 2002). Frictional models for dynamic

triggering will be limited to areas where the stress state on pre-existing crustal faults hovers below the Coulomb failure stress by less than the peak dynamic stress amplitude.

8.04.1.1 Coulomb failure under dynamic stresses

Under the Coulomb model for friction, brittle failure occurs when the combination of shear (τ) and normal stress (σ) components on a fault plane exceed the cohesive strength, C, and the static coefficient of friction, μ_s, such that the Coulomb failure function (equation 2) $CFF \geq 0$. In a Mohr's diagram (Figure 5A), $CFF = K_i$ a constant, forms a family of straight lines of with slope, μ with CFF = 0 representing Byerlees' law for frictional failure. $\Delta CFF = \Delta\tau - \mu\Delta\sigma$ (equation 1) is thus the interval between two lines, K_{i+1} and K_i . In the stable domain ($CFF < 0$), a positive ΔCFF indicates that the stress state has moved incrementally toward failure. Under the Coulomb failure model for dynamic triggering (Figure 5B), the traction $\mathbf{T}[R(t), \theta(t)]$ on a fault at angle θ with respect to the initial stress state, $\mathbf{T}_1$, begins an oscillatory trajectory as the seismic waves arrive at time t_0. A triggered earthquake results if the trajectory enters the Coulomb failure zone $CFF \sim 0$ (grey band in Figure 5). The stress drop associated with the triggered earthquake alters the stress state (its orientation, θ, and the stress difference, $R_2 < R_1$) in the vicinity of the fault such that the traction on the fault settles to a new value, $\mathbf{T}_2$, after the seismic waves have passed ($t > t_d$). Multiple earthquakes may occur during a single dynamic stress cycle if the initial triggered earthquake produces its own aftershock sequence or if the stress cycle triggers earthquakes on multiple nearby faults. A particularly compelling example of this behavior is illustrated in Figure 8 where bursts of small, earthquakes at Mt. Wrangell, Alaska, occur in phase with peaks in the horizontal extensional stresses during the Rayleigh wave train from the M_W =9.1 Sumatra-Andaman Islands earthquake of 26 December 2004 (West et al. 2005).

<Figure 8 near here>

In principle, this model should be viable in any region where faults are critically stressed and favorably oriented with respect to the polarity of the dynamic stresses from a distant earthquake. If most of the seismogenic crust is pervasively fractured and critically stressed as suggested by (Zoback and Zoback 2002), earthquakes triggered by this process have an equal likelihood of occurring nearly everywhere. If this were the dominant triggering mechanism, one would expect that, given some minimum dynamic stress level, the distribution of observed triggered seismicity would correlate directly with density of seismic networks and sensitivity of earthquake detection techniques. As Rivera and Kanamori (2002) argue, however, heterogeneity of both the stress field and frictional strength seems to be an essential property of the crust. In a similar vein, Lapusta and Rice (2003) argue for heterogeneous strength along a given fault such that earthquake nucleation is confined to weak spots while the average fault strength remains well above the Coulomb failure threshold.

8.04.1.2 Non-linear friction

Extensive laboratory experiments on rock friction reveal that frictional failure involves a much richer range of (non-linear) behaviors than predicted by the familiar first-order model involving a constant static μ_s and dynamic μ_d coefficients of friction with $\mu_s > \mu_d$. The Dieterich-Ruina rate-state friction laws (Dieterich 1979) have been widely used in studies of both static and dynamic triggering. These rate-state laws, in which static friction retains a memory of sliding history along the fault surface and dynamic friction depends on the sliding velocity and an evolving state parameter, predict a range of behaviors depending on temporal variations in the applied stress and the parameter regime for the constituative relation (Dieterich 1979, Scholz 1998). In the unstable, velocity-weakening regime, for example, rate-state friction appears to be most effective under conditions of low effective normal stress (high pore pressure and weak faults) together with high-frequency vibrations (high stressing rates) (Gomberg et al. 2003, Perfettini et al. 2003, Scholz 1998). Brodsky and Prejean (2005) however, conclude that near-lithostatic pore pressures would be required for the rate-state friction model to be consistent with the dynamic triggering observed in Long Valley caldera. To first order, then, rate-state friction offers no significant advantage over the simple Coulomb failure model for the onset of stick-slip (seismicity) under dynamic triggering. Because the frictional state is changed by slip, however, the rate-state model admits the possibility of an Omori-like decay of triggered seismicity after shaking has stopped (Gomberg et al. 2005).

One interesting implication of rate-state friction in the conditionally stable regime is that dynamic stresses can temporarily convert stable sliding (steady fault creep) to a stick-slip mode. As discussed by Gomberg et al.(1997), this represents "new seismicity" in the sense that the earthquakes generated during the stick-slip mode would not have occurred in the absence of dynamic triggering. This model may apply to Stierman's (1977) recordings of acoustic emissions in a borehole within creeping section of the San Andreas fault near Parkfield as the seismic waves from the underground nuclear explosion KASSERI passed through the area on 28 October 1975.

Experiments by Johnson and Jia (2005) on the response of granular media to imposed dynamic stresses offer insight on another possible mode of nonlinear frictional failure. They find that seismic waves with peak strain amplitudes greater than $\sim 10^{-6}$ (or $> \sim 0.03$ MPa) incident on a weak fault with a core composed of fault gouge (the granular medium) can result in an abrupt decrease in the modulus of the fault gouge. Their experiments show that for faults with effective normal stresses less than ~ 1 bar (e.g. near lithostatic pore pressures) and a near-critical shear stress, the result can be catastrophic slip and an earthquake (Johnson et al. in press).

8.04.1.3 Subcritical Crack Growth

Subcritical crack growth or stress corrosion is a process that has long been known in material science to make cracks unstable (Anderson and Grew 1977, Atkinson 1984, Gomberg et al. 2001). When a crack experiences a change in its environment, such as a sudden increase in loading in the presence of particularly high temperatures and fluids, it may grow due to weakening at the crack tip by chemical corrosion. The crack may then

rupture catastrophically. Thus, a sudden increase in loading or oscillatory loading (dynamic stressing) may shorten the time to earthquake failure. The equations governing subcritical crack growth are mathematically identical to those governing failure by rate and state friction (Kanamori and Brodsky 2004), and thus, as Brodsky and Prejean (2006) point out, sub-critical crack growth requires near-lithostatic pore pressures to be effective as a dynamic triggering process.

Because each of the above non-linear models (rate-state friction, granular media, and sub-critical crack growth) apparently requires near-lithostatic pore pressures to be effective in dynamic triggering (Brodsky and Prejean, 2006), it seems unlikely that they offer a universal explanation for dynamic triggering. Any of the three, however, may be important in limited volumes of the crust where pore pressures approaches the lithostatic limit.

8.04.2 Triggering Through Excitation of Crustal Fluids

Crustal fluids play a critical role in a wide range of tectonic and magmatic processes (see Chapter 11 on earthquake hydrology by M. Manga), and there is no reason to suppose that dynamic triggering should be an exception. Large earthquakes have long been recognized as capable of disturbing hydrologic regimes at distances of thousands of kilometers beginning with the $M_W = 9.2$ 1964 Alaska earthquake (Vohis 1967, Roeloffs 1996), and fluids have long been known to play a role in earthquake rupture (e.g. Nur and Booker 1972). These observations have inspired a class of physical models in which dynamic strains from the distant earthquake trigger local seismicity through fluid transport and pore pressure changes. This process may modify the Coulomb failure function (section 8.04.1.1) such that the effective normal stress is decreased sufficiently to trigger failure (Beeler et al., 2000; Cocco and Rice, 2002) or that quasi-static (aseismic) strains associated with local, fluid-driven deformation are sufficient to trigger earthquakes. Fluids are active agents in geothermal and volcanic areas, which appear to be particularly susceptible to dynamic triggering, and a number of explanations for triggered seismicity involving the movement of fluids have been proposed in the literature (e.g. Brodsky et al. 1998, Linde et al. 1994, Moran et al. 2004, Johnston et al. 1995, Hill et al. 1995).

In geothermal and volcanic areas, the simple linear version of "clock advance" may be compromised because, in addition to steady loading from far-field tectonic stresses, advection of fluids and heat from lower crustal or upper mantle source supply local energy into a recently triggered volume of the brittle crust. As is evident from the behavior of the Long Valley caldera volcanic-geothermal system over the past 25 years, these processes may operate episodically over time scales ranging from weeks to years (Hill in press).

8.04.2.1 Hydrous fluid transport: changes in permeability and pore pressure

In this class of models for earthquake triggering, the dynamic strains from a distant earthquake modify crustal permeability by disrupting clogged fractures and hydraulic

fracturing, thus leading to a redistribution of pore pressure. These models should be viable in any area where isolated pockets of high pressure fluids develop. Brodsky et al. (2003) for example, proposed that co-seismic water level changes observed in wells at Grant's Pass in southern Oregon might result from dynamic stresses from M=7.2 and M=7.4 earthquakes at ~300 km ~3,850 km, respectively, opening permeable fractures clogged by accumulating detritus over time.

The pore pressure redistribution mechanism may be particularly relevant in active geothermal areas, such as the Geysers and Coso geothermal fields, as fractures are sealed and high pressure compartments form over relatively short time scales as minerals are precipitated from hot brines. The mechanism may also be important in the crust above a magma body in which hydrous magmatic fluids may reach near-lithostatic pressures in the low-permeability plastic zone between the roof of the magma body and the brittle crust, where hydrothermal fluids circulate under hydrostatic conditions. This is the hydraulic surge model proposed by Fournier (1999) in which dynamic stresses from a large distant earthquake may rupture this impermeable zone, permitting high pressure fluids to surge into the overlying brittle crust. This mechanism may explain both earthquakes triggered during and after the wavetrain of the large distant earthquake has passed as pore fluids move by diffusion through the crust.

Hough and Kanamori (2002) looked for evidence of fluid movement in the failure process of earthquakes triggered in the Salton Sea by the 1999 Hector Mine earthquake by examining earthquake source parameters. They found that the triggered earthquakes had essentially normal to slightly low stress drops and spectral contents typical of brittle shear-failure with no resemblance to the long-period earthquakes or tremor-like sequences often seen in volcanic areas (Chouet 1992, Julian 1994, Julian,1992). As pointed out by Brodsky and Prejean (2005), earthquakes triggered by pore pressure increases would not necessarily have a signature of active fluid involvement in the source process, as increased pressure may simply decrease normal stress, leading to standard shear failure.

8.04.2.2 Magmatic fluids

Growing evidence indicates that dynamic stresses are capable of perturbing the state of crustal or upper mantle magma bodies triggering internal pressure changes and, in some cases, eruptions (Hill et al. 2002, Manga and Brodsky 2005, Linde and Sacks 1998, Marzocchi 2002). Under these models, triggered seismicity is a secondary result of locally triggered deformation associated with the change in state of a nearby magma body. Because these models predict distinctive patterns of ground deformation associated with triggered seismicity, continuous high-resolution deformation monitoring networks will be needed to test them.

8.04.2.2.1 Bubble excitation

One intriguing class of models proposed to explain earthquake-magmatic interactions centers on the role of bubbles in magma. Bubbles play a central role in the source

mechanisms for long-period and very-long-period volcanic earthquakes (Chouet 1992) as well as in eruption dynamics (Mangan and Sisson 2000). Two highly idealized physical models widely mentioned as possible explanations for remotely triggered seismicity appeal to changes in bubble pressurization in a two phase fluid. In the rectified diffusion model, volatiles in a saturated fluid are selectively pumped into bubbles during the dilatational phase of each strain cycle as the wavetrain of the distant earthquake passes (Sturtevant et al. 1996, Brodsky et al. 1998). Increasing pressure in the bubbles is transmitted to the surrounding interstitial fluid, thereby increasing pore pressure and triggering earthquakes. In the advective overpressure model, bubbles adhering to the rigid walls of a magma body are shaken loose by the dynamic strains from the remote earthquake. As these bubbles rise a distance, h, through the (incompressible) magma, pressure in the magma chamber increases by ρgh (where ρ is magma density and g is the acceleration of gravity) thereby deforming the surrounding elastic crust and increasing pore pressure in the surrounding brittle rock (Linde et al. 1994, Sahagian and Proussevitch 1992). In principle, both models could apply to either hydrous fluids or magma, although both have been criticized on the basis that they depend on restrictive assumptions that are unrealistic under natural conditions in the Earth (Pyle and Pyle 1995, Brodsky et al. 1998, Bagdassarov 1994, Ichahara and Brodsky, 2006).

Manga and Brodsky (2005) explore what appears to be a more realistic model for the role of bubbles in dynamic triggering based on the creation of new bubbles (bubble nucleation) in a supersaturated magma. They conclude that, under proper conditions, small pressure changes associated with dynamic stresses in a crystallizing magma that is close to critical supersaturation should be capable of triggering a significant excess in bubble nucleation leading to a marked pressure increase. Numerical modeling by Shimomura et al. (2006) and Chouet et al. (in press) indicates that a densely packed matrix of tiny bubbles in a magma-filled crack when subject to a small, externally imposed pressure drop can lead to rapid diffusion-driven bubble growth and volumetric expansion of the crack. These models have yet to be evaluated for their response to realistic dynamic stresses, but they keep open the possibility that bubbles may have an important role in the triggered response of magmatic systems to dynamic stresses.

8.04.2.2.2 Magmatic intrusions

Dilatational strain meters at Mammoth Mountain recorded deformation transients coincident with the seismicity triggering in the Long Valley caldera area following the Landers, Hector Mine, and Denali Fault earthquakes. Based on these data, Johnston (2000) and Johnston et al. (2004a) have proposed that in the case of Mammoth Mountain and Long Valley, the dynamic waves from distant earthquakes trigger magmatic intrusions into the shallow crust. These intrusions, which may involve a massive hydrofracture by aqueous magmatic fluids or magma itself, then trigger earthquakes by changing the static stress field or locally increasing the pore pressure as fluids are exsolved. Thus the local seismicity is a secondary response to the initiating ground motion.

8.04.2.2.3 Relaxing Magma Body

Dynamic waves from a large distant earthquake may disrupt the stability of a partially crystallized magma body releasing accumulated deviatoric stress supported by the interconnected crystal structure (Hill et al. 1995). As in the magmatic intrusion model, the local seismicity triggered by a relaxing magma body is responding to a local, quasi-static strain source rather than the initiating dynamic stresses. The recharge time for this model is presumably rather long depending on both the crystallization rate in cooling magma body and the far-field strain rate. If such a model has any merit, it raises a question regarding the response of Long Valley Caldera to the M = 7.6 Owens Valley earthquake of 1872, which ruptured to within 50 km of the caldera based on this model. Did the static stress change from the Owens Valley earthquake load strain energy into to the crystalline matrix of crystallizing magma body that was subsequently released by dynamic stresses from the 1992 Landers earthquake? If not, the validity of the model as an explanation for the Landers deformation transient is in doubt. Indeed, it seems unlikely that a crystalline matrix could reform sufficiently rapidly to accumulate significant elastic strain in the intervening 120 years if shaking from the Owens Valley earthquake disrupted the magma body in 1872.

8.04.2.2.4 Sinking Crystal Plumes

Another possible response of a mama body to dynamic stresses suggests that passing seismic waves may dislodge dense crystals from the ceiling and walls of a magma chamber. As these crystals then sink due to gravity, they may stimulate convection in the magma chamber. Bubbles would presumable nucleate and grow in the ascending volatile rich magma thereby increasing pressure in the magma body and deforming the overlying crust (Hill et al. 2002). Manga and Brodsky (2005) show that this process may be capable of creating sufficient overpressure to trigger a volcanic eruption on the time scale of days. Thus it is likely the process could trigger earthquakes on a similar time scale, although such calculations have not yet been performed.

8.05 CHALLENGES FOR THE FUTURE

The study of remotely triggered seismicity gives us a unique window into the earthquake nucleation process, as it is the only naturally occurring example where we know precisely what perturbation to the Earth's stress field triggered an earthquake. Although this is a fertile field of study with great potential for illuminating the earthquake initiation process, many fundamental questions remain regarding the detection, temporal and spatial distribution, and physical processes behind dynamically triggered seismicity.

8.05.1 Challenges in Detecting Triggered Seismicity

Although identifying triggered earthquakes can be straight forward in the case of an abrupt increase in seismicity (e.g. Figures 2, 6, 7), it is likely that many earthquakes triggered by dynamic waves remain undetected. Swarms of earthquakes are far easier to link to the remote earthquake than isolated earthquakes. Whether the two earthquakes offshore of CA event following the Denali Fault Earthquake (Prejean et al. 2004) is a

triggered event or not remains a vexing question of statistical significance. Also, as the time separation between the onset of the dynamic wavetrain and the triggered earthquake increases, it becomes increasingly difficult to show statistically that the two are linked.

When triggered earthquakes occur in swarms, we are faced with the problem of distinguishing between triggered earthquakes and aftershocks to the triggered earthquakes (Ziv, 2006). One promising approach to this problem involves the epidemic-type aftershock sequence (ETAS) model described by Hainzl and Ogata (2005) to distinguish earthquakes driven by external forcing (such as fluid transport) from those resulting from an Omori-type aftershock sequence. High-resolution imaging of spatial-temporal patterns of swarm evolution can also provide evidence for fluid forcing, particularly when the seismicity front propagates as ($r/\sqrt{t}$) characteristic of fluid diffusion (Shapiro et al. 1997). This approach should be particularly useful in tests for Fournier's (2000) hydraulic surge model, which implies an upward propagating seismicity front driven by fluid diffusion.

Another challenge we face is discriminating dynamically triggered earthquakes from those triggered by static and quasi-static process. To avoid this uncertainty many researchers have limited their data sets to events triggered at distances greater than ~2 fault lengths from the mainshock where static stress changes become too small to trigger earthquakes (Hill et al. 1993). However, as Gomberg et al. (2003) suggested, we may be severely limiting our data set by overlooking dynamically triggered earthquakes within the aftershock zone even though static stress triggering also plays a role in this realm (King et al. 1994). By comparing dynamic stress amplitudes with the aftershock distribution, Kilb et al. (2002) have shown that many aftershocks are probably dynamically triggered. More recently, Feltzer and Brodsky (2006) show that the density of aftershocks with distance from a mainshock is directly proportional to the dynamic stress amplitudes from the mainshock at those distances. Pollitz and Johnston (2006) find that slow (quasi-static) earthquakes in central California have many fewer aftershocks than typical brittle-failure earthquakes of comparable moment. These studies indicate that dynamic waves may play a much larger role in triggering early aftershocks in the near field than was previously suspected.

Finally, automated earthquake detection algorithms are ineffective at identifying small triggered events recorded by a single, low-dynamic-range station. Reliable identification of triggered seismicity buried in the surface wave coda from a large earthquake requires either visual scanning of high-pass filtered signal or a spectrogram display as illustrated in Figure 6 (e.g. Prejean et al. 2004). This capability is unevenly distributed in existing seismic networks.

8.05.2 Challenges in Mapping the Distribution of Triggered Seismicity

Detailed investigations of triggered seismicity following the Denali Fault Earthquake showed conclusively that triggering by dynamic seismic waves is probably far more common and widespread than was previously recognized. Prior to the Denali Fault Earthquake, triggered seismicity was primarily identified through abrupt seismicity rate

increases in earthquake catalogs following a large distant earthquake (e.g. Figure 2, 7). In the case of the Denali Fault Earthquake however, hundreds to thousands of triggered earthquakes did not appear in earthquake catalogs, either because they were masked by the mainshock coda when many instruments are saturated and automatic earthquake detection algorithms do not work, or because they were too small to be seen at more than one station (Gomberg et al. 2004, Prejean et al. 2004, Pankow et al. 2004, Husker and Brodsky 2004). The installation of many broadband, high dynamic range instruments in the last decade has allowed scientists to identify high frequency local earthquakes in the relatively low frequency wavetrain of the Denali Fault Earthquake at many new sites (Figure 6). In many places however, limitations in dynamic range continue to limit our ability to search for triggered events during the mainshock's wavetrain.

Many lines of evidence suggest that areas with higher background seismicity rates are more likely to experience dynamic triggering than areas with lower background seismicity rates because these areas are more frequently closer to failure (see section 8.03.1.1). Because areas with high seismicity rates tend to be densely instrumented however, we are more likely to catch triggering in those areas. This highlights the question: to what degree is our current picture of the distribution of remotely triggered seismicity real or the result of a bias due to variations in network density? Spatial variations in network density compound the potential lack of conformity in earthquake triggering maps.

Many more cases of remote dynamic triggering have been observed in geothermally and/or volcanically active areas and areas undergoing active crustal extension than in other tectonic regimes (see 8.03.1.1 and Table 2*)*. Whether these observations are an artifact of high background seismicity rates, high network densities, or high levels of scrunity in these areas has not been thoroughly addressed in the literature and remains an open question. Based on case studies, Spudich et al. (1995) suggest that remote triggering is less common in compressional and trantensional non-geothermal areas (specifically along the San Andreas fault) than in geothermally active areas, even when the background seismicity rates, network densities, and levels of scrutiny are compatible. A systematic study of the occurrence of triggering over large areas (such as the tectonically active western United Sates or the more stable mid-continent) that includes more recent and complete observations has yet to be done.

8.05.3 Challenges in Determining the Ttriggering Processes

In the last two decades many intriguing physical models have been proposed to explain remotely triggered seismicity. Some of these models are highly quantitative and testable in the right circumstances; others have not left the realm of thought provoking but untested speculation. Ror this field to advance, we must find ways to quantify and constrain these models.

To determine the physical processes responsible for a remotely triggered earthquake, we need thorough knowledge of the triggering wave field in space and time, precise hypocentral locations for the triggered seismicity, focal mechanisms, and other source

properties as well as the physical environment where triggering occurs (fault orientations, frictional properties of faults, stress field and hydrologic regime). Earthquakes that are triggered during the mainshock wave train (Figure 6) provide a promising opportunity to investigate failure processes because we can extract information on the spatial-temporal properties of the dynamic stresses at the time triggering is initiated.

The idea that remote triggering depends on a simple amplitude threshold or a distance-magnitude threshold has yet to prove useful (e.g. Gomberg et al. 2001, Moran et al. 2004). Anderson et al., (1994) suggested that large, distant earthquakes trigger seismicity more readily than smaller more local earthquakes. The M_W = 6.4 Chalfant Valley earthquake of June 1986, for example, did not trigger seismicity in Long Valley caldera or Mammoth Mountain at a distance of just 20 to 30 km despite peak amplitudes much higher than more distant events that did lead to triggering. This suggests that the propensity for earthquake triggering may depend on frequency of shaking in addition to amplitude. Brodsky and Prejean (2005) show that in the case of Long Valley and Mammoth Mountain, earthquakes are generally triggered at remote distances more easily by low frequency surface waves (periods 15 to 30 seconds) than high frequency. In contrast, Gomberg et al. (1996) argued that triggering at the Geysers, CA, depended on high-frequency waves. This conclusion in their 1996 paper, however, was partially based on lack of evidence at the time for tidal triggering at periods of 12 to 24 hours (see section 8.02.5.3) compared with triggering by surface waves at periods of 15 to 30 seconds (Brodsky and Prejean 2005). As of mid 2006, the Geysers, CA, Katmai, AK, and Long Valley Caldera- Mammoth Mountain, CA, are the only sites that have multiple examples of triggering and non-triggering dynamic stresses to test these hypotheses. Of these, only the Long Valley caldera area has broadband instrumentation capable faithfully recording ground motion spanning a wide dynamic range and over a wide frequency spectrum. As more triggering observations are made and more broadband, high-dynamic-range data become available, it is likely we will make progress in addressing this question.

West at al. (2005) show that in the Sumatra-Andaman Islands earthquake of 2004, earthquakes were triggered at Mt. Wrangell, Alaska only during the large positive vertical displacements of the Rayleigh wavetrain (Figure 8). Thus, they were able to calculate the specific strain at the general location of the earthquakes at the time of triggering and conclude that these observations would be consistent with triggering by simple shear failure on normal faults. With the limited available data, however, focal mechanisms of the triggered earthquakes could not be resolved.

Estimating the character of the dynamic wave field at the hypocenter of a triggered earthquake requires extrapolation in three dimensions from recordings at nearby stations. (e.g. Gomberg and Davis 1996). Many triggered earthquakes are small and lack reliable focal mechanisms, so even if we understand the dynamic ground motion at the site of triggering, we do not know how that strain field affected the particular failure plane as is the case in of the Wrangell triggering (West et al. 2005).

A number of informative studies using existing data could be conducted to test individual models for the physical process leading to dynamic triggering. Specific parameters for models based on rate and state friction might be tested by analyzing the decay rate of triggered events and searching for changes in rates of background seismicity after episodes of triggering.

Although strain transients have been observed in every episode of triggering when continuous, high-resolution strain data are available, whether these strain changes are an intrinsic part of the triggering process remains unknown. Inferences about magmatic intrusion and relaxing magma bodies are based on strain data (e.g. Linde et al. 1994, Sturtevant et al. 1996, Johnston et al. 2004a). To test these models it is imperative that we have strain data in more locations and higher densities of strain networks, so we can adequately model the deformation source. Strain data are key in testing models that involve fluid transport. However, it is difficult to tell at this time whether strain signals are reflecting a compact or a distributed source, such as a regional pore pressure change (Segall et al. 2003). High frequency water well data will also be helpful in testing models that involve crustal fluid flow and pore pressure changes (Roeloffs 1996), as these data can help determine how the crust responds hydrologically to large distant earthquakes.

Finally, in considering these models we must also recognize that there may be no one unifying causative process. Rather a range of triggering mechanisms may be valid in different locations, over different time scales. In the case of Long Valley for example, a swarm of earthquakes <M1 that occurred under Mammoth Mountain by the Denali Fault dynamic stresses were likely triggered by a different process than a swarm of M<=3 earthquakes that began 24 hours later, 10 km to the east in the caldera's south moat. Thus testing individual models against large data sets that cover a variety of physical environments, distances, and time scales may not prove successful.

8:06 CONCLUSIONS

The question is no longer whether seismic waves (dynamic stresses) from large earthquakes are capable of triggering local earthquake activity over distances ranging from tens to thousands of km; the evidence in support of dynamic triggering as a common phenomenon is compelling. Rather, key questions have become: what conditions favor dynamic triggering, and what physical processes do dynamic stresses induce in given crustal volumes that trigger local earthquakes and, at least in some cases, local deformation? To a large degree, emerging answers will come into focus as we obtain more complete sampling of the triggered response to future large earthquakes in terms of both spatial distribution and variations in response characteristics over a wide spectrum of time scales afforded by more widely distributed broad-band seismic and continuous deformation instrumentation.

Based on the still woefully uneven sampling available through mid 2006, it appears as though tectonically active extensional regimes (such as the Basin and Range province in the western United States with strain rates of ~10^{-8} y^{-1}) are more susceptible to dynamic triggering than stable cratonic regimes (such as the eastern United States with strain rates generally < 10^{-9} y^{-1}). Higher tectonic strain rates mean shorter recovery (recharge) times between episodes of strain release (whether dynamically triggered or not). In volcanic and geothermal areas, recovery times may be further shortened by episodic advection of thermal fluids into the crust from the lower crust or upper mantle that serve as local stress sources. Shorter recovery times mean that, at any give time, more areas are likely to be hovering in a near-critical state and thus susceptible to triggering by small dynamic stresses than in areas with low strain rates and extended recovery times. As Hough et al. (2003) argue, however, non-elastic deformation in mid-continental low strain-rate environments should act maintain stresses at a near-critical state failure for longer periods than in high strain-rate environments such that a dynamic stress change can lead to a relatively large clock advance. We have yet, however, to see clear examples of remote dynamic triggering in the central or eastern sections of the United States recorded on modern seismic networks.

In any case, elevated strain rates alone are not sufficient. The central section of the San Andreas Fault through the California Coast Ranges with its high strain rate (~$5x10^{-7}$ y^{-1}) and frequent seismicity appears not to be particularly susceptible to dynamic triggering (Spudich et al. 1995). One explanation for this apparent difference in triggering susceptibility appeals to the importance of vertical mobility of crustal fluids in the dynamic triggering process. Fluid-filled cracks open in the direction of the least compressive stress and thus tend to have vertical orientations in extensional regimes and horizontal orientations in transpressional regimes such as that along the San Andreas Fault. Whatever the case, currently available data are not adequate to clearly distinguish between the many competing models for the triggering process, which range from various formulation of friction to hydrous fluid transport or the excitation of magma bodies. Models involving the activation of fluids or the transition to a frictional domain of stable sliding admit the possibility that triggered seismicity is a response to some form of local, aseismic ground deformation, which underscores the importance of obtaining continuous deformation data in areas susceptible to dynamic triggering.

Models proposed to explain dynamic triggering fall into two broad categories: 1) frictional models tied to the Coulomb failure function and direct triggering of local seismicity, and 2) models that appeal to the excitation of local crustal fluids or aseismic creep with seismicity developing as an indirect (and possibly delayed) response. For dynamic triggering under the frictional models, the stress state in the crust must differ from the Coulomb failure stress by less than the peak amplitudes of the dynamic stresses (typically < 0.1 MPa for remote triggering). These models are generally consistent with the onset of triggered seismicity during the dynamic stresses followed by an Omori-like decay depending on the parameters for the specific friction law (e.g. rate-state, granular media, etc.).

Fluid excitation models involve fluid transport or a phase change driven by the triggered release of locally stored gravitational or chemical potential energy. These fluid-based models, whether hydrous or magmatic, together with models based on aseismic creep, involve some degree of crustal deformation through, for example, intrusion, pressure changes in the case of bubble excitation, advection in a magma body, or poroelasticity in the case of fluid diffusion. Triggered seismicity for many of these models can be a secondary response to quasi-static stresses generated by local deformation, and thus they are somewhat less dependent on a near critical stress state than the friction models. These models admit the possibility of delayed onsets of triggered seismicity and increasing or sustained activity rates for extended periods following passage of the dynamic stresses. Confidence in delay times $\Delta t >> 3/\lambda$ (Appendix I), however, will depend on the existence of a compelling physical model. In general, fluid-based models are more likely to the more applicable in extensional stress regimes that host geothermal and volcanic systems than to stable regimes. Of course nothing precludes a triggering episode from being the result of some combination of frictional and fluid-based models.

Finally, because the three-dimensional dynamic stress fields for seismic waves from large earthquakes or solid Earth tides can be calculated with reasonable accuracy, they serve as potentially powerful tools for investigating the state of stress in the crust and what it means to be in a near-critical state as well as insight on complex rupture processes through near-field dynamic triggering of nearby large earthquakes.

Acknowledgements
We are grateful to Emily Brodsky, Jeannie Hardebeck, Sue Hough, and Jim Mori for constructive reviews of early version of this manuscript and to Hiroo Kanamori for his guidance as volume editor. Special thanks to Paul Reasenberg for his thoughtful insight on the application of the beta statistic to dynamic triggering.

APPENDIX I. Statistical significance

The β-statistic (Matthews and Reasenberg 1988, Reasenberg and Simpson 1992) is widely used in the literature as a test for statistical significance in instances of suspected dynamic triggering. In this appendix, we focus on the β-statistic as means of illustrating some important issues associated with evaluating the statistical significance of dynamic triggering and we note some alternative approaches where appropriate. This appendix is not intended to be an exhaustive survey of statistical tests for dynamic triggering.

Mathhews and Reasenberg (1988) developed the β-statistic as a test for the statistical significance of an offset in average background seismicity rates associated with static stress changes due to a nearby earthquake under the assumption that background seismicity is a Poisson process. The value of β produced by this test represents the number of standard deviations by which the seismicity rate, $r_a = n_a/t_a$, in a given area after a mainshock of interest differs an estimate of the background seismicity rate $r_b = n_b/t_b$, prior to the mainshock. Here, n_a and n_b are the number of earthquakes during the

time intervals t_a and t_b after and before the mainshock, respectively. Reasenberg and Simpson (1992) express the β-statistic as

$$\beta(n_a, n_b, t_a, t_b) = [n_a - E(n_a)] / [var(n_a)]^{1/2}$$

where $E(n_a) = r_b t_a = n_b(t_a / t_b)$ is the expected number of earthquakes during t_a based on a sample of the background seismicity during t_b, and $var(n_a)$ is the variance. For a Poisson process, $var(n_a) = r_b t_a$. The β-statistic is commonly evaluated over an array of spatial bins to create a β-statistic map as in Figure 3. Results with $|\beta| > 2$ (approximately two standard deviations) are generally considered to be statistically significant (Reasenberg and Simpson 1992).

As with any statistical test, however, it is important to recognize the assumptions behind the test and to insure that the same assumptions are consistent with the data at hand. It is equally important to have a clear idea of the hypothesis being tested. The β-statistic was developed to test the hypothesis of a change (either increase or decrease) in average seismicity rate at time t_0 against the null hypothesis of no significant rate change, where t_0 marks the transition from t_b to t_a. In the case of dynamic triggering, we are more interested in the significance of a transient seismicity cluster beginning within some time interval $\Delta t < t_a$ following the onset of dynamic stressing at t_0. Accordingly, applying the β-statistic to putative cases of dynamically triggered seismicity requires some compromises.

One such compromise involves the choice made for the duration of post-mainshock interval, t_a. An overly long interval may contaminate the test by including background seismicity fluctuations not related to dynamic triggering while too short an interval may introduce problems associated with the statistics of small samples. This choice is unimportant to first order when applied to the detection of a step change in seismicity rate as originally intended because the rate is assumed to be constant after the mainshock. When applied to triggered seismicity, however, the choice of t_a, directly affects the calculation of $r_a = n_a/t_a$ and thus the value of β.

Strictly speaking, application of the original formulation of the β-statistic to the evaluation of triggered seismicity violates the assumption that seismicity in both intervals, t_a and t_b, reflects a Poisson process. The clustered seismicity typical of a triggered response might better be represented using the "epidemic-type aftershock sequence" (ETAS) model of Ogata (1993). Using short intervals for t_a in a β-statistic test for the significance of questionable instances of dynamic triggering may be particularly susceptible to unstable results considering that the Poisson distribution is valid for a large number of events, n, each with a small probability, p. In an effort to circumvent this problem, Pankow et al. (2004) proposed a test based the binomial distribution in their analysis of dynamically triggered earthquakes in Utah by the 2002 Denali Fault earthquake, and Gomberg et al. (2001), Kilb et al. (2002), and Hough (2005) use a modified form of the β-statistic incorporating the binomial distribution. In the end, however, results based on a small number of earthquakes should be viewed with caution.

Viable estimates of background seismicity rates, r_b and r_a, for the β-statistic as originally intended depends on the effective removal of aftershock sequences and earthquake swarms for the entire time interval ($t_a + t_b$) by running the earthquake catalog through a de-clustering algorithm such as that developed by Reasenberg (1985) or Hainzl et al (2006). Viable estimates of background rates also require a stable earthquake catalog with a well established completeness threshold (the minimum magnitude above which all earthquakes in the area are detected by the seismic network and included in the catalog) and reasonable assurance that any change in data processing has not introduced an offset in earthquake parameters such as magnitude and completeness threshold (Wiemer 2001, Wiemer and Wyss 2000). De-clustering the post dynamic stress interval, t_a, in a test for dynamic triggering, however, is likely compromise the signal of interest (the triggered seismicity cluster).

One of the more useful applications of the β-statistic to dynamic triggering involves developing a map showing the spatial distribution of likely instance of dynamic triggering as in Figure 3 (Gomberg et al. 2001). Choice of an appropriate bin size over which to evaluate the β-statistic is analogous to the choice of an appropriate post-mainshock time interval, t_a, both of which are typically under-constrained. The bin area should be sufficiently large to include a "reasonably large" number of earthquakes. As the area increases, however, spatial resolution decreases and the odds of including random fluctuations in background seismicity increase – particularly in regions with elevated background seismicity rates. Optimal bin size is likely to vary from one region to another depending on background seismicity patterns. One approach to this problem is to evaluate the sensitivity of β to bin size in a given region by calculating β over a range of bin sizes. Because the β-statistic is an imperfect test for dynamic triggering, however, prudence dictates that areas highlighted as possible sites of dynamic triggering be examined for independent evidence of a seismicity cluster beginning within some "reasonable" time interval Δt, following the dynamic stresses.

The delay time, Δt, between arrival of dynamic stresses from a distant mainshock and the onset of triggered seismicity is one of the more important parameters in dynamic triggering in that it provides clues on the triggering process. Although the onset of a suspected triggered response is often marked by a relatively clear increase in seismicity rate, the question of a reasonable upper bound on the time delay, Δt, remains. Clearly, delay times that approach the mean inter-event time for fluctuations in background seismicity rates in a given area beg the question of statistical significance. The β-statistic is of little use on this front. A conservative approach to this question is that applied by Paul Reasenberg to the triggered response to the 1992 Landers earthquake (see note 15 in Hill et al. 1993). He assumed that seismicity at a given site following a large, distant earthquake can be represented by a Poisson process with a rate, λ, and that the onset of the triggering process coincides with the origin time of the distant earthquake. Because inter-event times in a Poisson process are expected to exceed $3/\lambda$ just 5% of the time, the corresponding upper bound the delay time for statistically significant triggering becomes $\Delta t < 3/\lambda$. In the case of the Landers earthquake, Reasenberg estimated λ from the first ten earthquakes, $t_1 \ldots t_{10}$ following the mainshock origin time, t_o. He found $\Delta t = (t_1 - t_o) < 3/\lambda$ in 13 out of 14 instances with Δt ranging from 3 minutes (corresponding to the

surface wave propagation time) to 23 hours. It is important to note that 1) this approach does not rely on the β-statistic, 2) Reasenberg's choice of the first 10 events to define the rate is rather arbitrary, and 3) the triggered clusters were initially visually identified by their abrupt onset and high rate (Figure 2).

For additional statistical tests relevant to dynamic triggering, see for example, Marsan (2003), Ziv (2006), Harrington and Brodsky (2006) and references therein. Carefully applied, any of these tests offer an important aid in judging the validity of an inferred causal link between dynamic stresses from a distant mainshock and local seismicity rate increases. Blindly applied, of course, they can be seriously misleading. Clearly, any of these tests depend critically on the quality, duration, and completeness of local earthquake catalogs as a basis for establishing a reliable estimate of the background seismicity for the area of interest.

Table 1. Major earthquakes triggering multiple sites

Earthquake	magnitude	date	N sites	Max range	Trig Mmax	Ref.
Landers, CA	Mw=7.4	28-Jun-92	14	~1250 km	5.6	4
Hector Mine, CA	Mw=7.1	16-Oct-99	5	~750 km?		2, 3
Izmit, Turkey	Mw=7.4	17-Aug-00	Widespread in Greece	~1000 km	3.8	1
Denali Fault, AK	Mw=7.9	11-Mar-02	~18	>3660 km	3.2	6
Sumatra-Andaman Is	Mw=9.0	26-Dec-04	2	~11,000	< 2?	7, 8
Tokachi-oki	Mw=8.1	25-Sep-03	3	~1400 km	DLF*	5
SW Siberia	Mw=7.3	27-Sep-03	3	~4000 km	DLF*	5

*DLF – deep, low-frequency tremors

References: 1 (Brodsky et al. 2000); 2 (Glowacka et al. 2002); 3 (Gomberg et al. 2001); 4 (Hill et al. 1993); 5 (Miyazawa and Mori 2005); 6 (Prejean et al. 2004); 7 (West et al. 2005); 8 Ukawa, personal communication, 2005.

Table 2. Reported instances of remote dynamic triggering

Site	Responses		Regime	Triggering mainshocks		Ref.
	Number	Mmax		M min-max	Distance (km) min-max	
Mt. Wrangell, AK	1	M<1	V	9.1	~11,000	27
Katmai, AK	4	M=2.3	G, V	7.9	115 to 740	20
South B.C., Canada	1	N/A	C	7.9	1,800-2,200	8
Mt. Rainer, WA	1	M<1	V	7.9	3108	22
Geysers, CA	~11?	M<3	E, G, V	6.5 to 7.9	202 to 3120	6, 22
Coso, CA	>4	M=3.2	E, G, V	to 7.9	165-3,660	22
Long Valley, CA	2	M=3.4	E, G, V	7.4 to 7.9	414 to 3454	7, 22
Mammoth Mtn, CA	2	M<2	E, G, V	7.2 to 7.9	420 to 3454	2, 15
Lassen Peak, CA	1	M=2.8	E, V	7.4	840	10
Burney, CA	1	M=2.8	E	7.4	900	10
Salton Sea area, CA	1	M=4.7	E, V, G	7.1	120-150	13
Central & south CA	>5	M=5?	E & C	5.8 to 6.1	70-120	12
Offshore S. CA	1	M=2.5	E	7.9	4,003	22
Western Nevada	1	M~4	E, G	7.4	450-650	1
Little Skull Mtn, NV	1	M=5.6	E	7.4	240	1
Yellowstone, WY	2	M=3.0	E, G, V	7.4 to 7.9	1250 to 3100	14
Wasatch front, UT	2	M=3.2	E, G	7.4 to 7.9	3,000-3,500	21
Cascade, ID	2	M=1.7	E, G	7.4	1,100	8
Eastern US (1811-12)	1	M~5?	C	M>7	~1,000	12
Cerro Prieto, Mexico	1	M=4.1	E, V, G	7.1	260	5
Valley of Mexico	~7	M~4	E, G, V	7.6 to 8.0	303 to 588	23
Aso, Japan	5	M~2	E, V	7.1 to 7.7	900-2213	17
Iwo Jima, Japan	4	M<2	IA, G, V	7.1 to 8.0	1228 to 2002	25
SISZ, Iceland	1	M~5	E, G	6.5	80-100	2
Roer Valley, Holland	1	M=3.7	E	5.4	40	4
Greece	1	M>3.5	E	7.4	400-1,000	3
Syria-Lebanon border	1	M=3.7	C	7.3	500	19
Tiawan region	9	M>4	?	6.5 to 7.1	138 to 2959	25
Nanki Trough, Japan	2	N/A	S	7.3-8.1	900-4,000	18
Tonga trench	2	M=5.9-7.7	S	7.1-7.6	260-290	23

Tectonic regimes: E – extensional, transtensional: C – convergent, transpressional; G – geothermal, V – volcanic, IA Island Arc; S -- Sub-crustal subduction zone; SISZ – South Iceland Seismic Zone.

References: 1 (Anderson et al. 1994); 2 (Arnadottir et al. 2004); 3 (Brodsky et al. 2000); 4 Camelbeeck et al. 1994); 5 (Glowacka et al. 2002); 6, (Gomberg 1996); 7 (Gomberg et al. 2001); 8 (Gomberg et al. 2004); 9 (Hill et al. 1993); 10(Hill et al. 1995); 11 (Hough 2001); 12 (Hough 2005); 13 (Hough & Kanamori 2002), 14 (Husen et al. 2004b); 15 (Husker and Brodsky 2004); 16 (Johnston et al. 2004b); 17 (Miyazawa et al. 2006); 18 (Miyazawa & Mori 2005); 19 (Mohamad et al. 2000); 20 (Moran et al. 2004); 21 (Pankow et al. 2004); 22 (Prejean et al. 2004); 23 (Singh et al. 1998); 24 (Tibi et al. 2002); 25 (Ukawa et al. 2002); 26 (Wen et al. 1996), 27 (West et al. 2005).

Figure captions.

Figure 1. Diagram from Kilb et al. (2000) illustrating differences between static and dynamic stresses with distance in terms of idealized time histories for peak changes in dynamic (*ΔCFF(t)*) and static (*ΔCFF*) Coulomb stress. *ΔCFF(t)* is the time-dependent version of *ΔCFF* (equation 1). The double arrows show peak values for *ΔCFF(t)* and *ΔCFF*. Adopted from *Nature* with permission.

Figure 2. Evidence for remote dynamic triggering by seismic waves from the M_W = 7.4 Landers, CA, earthquake of 28 June 1992 in a plot of cumulative number of locatable earthquakes at 11 sites in the western United States for 211 days beginning with 1 January 1992 (Hill et al. 1993). Numbers in parentheses are distances in kilometers from the Landers epicenter. Numbers at the right indicate the total number of earthquakes in the respective areas for the entire time interval. The short vertical bars at day 114 mark the M_W = 7.1 Petrolia earthquake of 25 April 1992 and those at day 180 mark the M_W = 7.4 Landers earthquake (reproduced from *Science* with permission).

Figure 3. β-statistic maps illustrating seismicity rate increases associated with the M_W = 7.1 Hector Mine earthquake of 16 October 1999 (A) and the M_W = 7.4 Landers earthquake of 28 June 1992 (B) from Gomberg et al. (2001) .The plots show a spatially smoothed β-statistic over dimensions of 20 km for $M \geq 2.0$ earthquakes from the Northern California Seismic Network (NCSN) and Southern California Seismic Network (SCSN) catalogs. The rate change was calculated for a two-week period following the respective mainshocks with respect to the background period 1987 through mid-1992 (pre-Landers). Thin lines are major fault traces. Circles in (B) mark sites of activity triggered by the Hector Mine earthquake. M5 in (B) reflects aftershock activity to a M=5.3 earthquake that occurred ~2.5 months prior to the Hector Mine earthquake. G = the Geysers geothermal area, LV = Long Valley caldera, SG = San Gorgonio pass, LSM = Little Skull Mountain (modified from *Nature* with permission).

Figure 4. Map showing sites with triggered seismicity in western North America from the Landers (green triangles), Hector Mine (blue circles), and Denali Fault (red crosses) earthquakes. Mainshock ruptures indicated by corresponding colored lines with arrow indicating rupture direction. Inverted gold triangle is Mt. Wrangell volcano, which showed a seismicity decrease following the Denali Fault earthquake (Sanchez and McNutt 2004) but responded to dynamic stresses from the M_W = 9.1 Sumatra-Adaman Islands earthquake of 26 December 2004 with several brief bursts of triggered seismicity (West et al. 2005)

Figure 5. (A) Mohr's diagram comparing maximum stress levels for extensional (normal faulting) and compressional (thrust faulting) regimes in a pervasively faulted crust with a common (e.g. hydrostatic) pore pressure and with frictional strength

limited by the Coulomb failure criteria (CFF = 0). τ and σ are the shear stress and effective normal stress components, respectively, acting on a fault plane at an angle, θ, with respect to the least principal stress, σ_3. The coefficient of static friction for rocks is $\mu \sim 0.6$ and C is the cohesive strength with the grey band representing scatter in data. The effective normal stress $\sigma = (\sigma_n - P)$, or the rock matrix normal stress σ_n reduced by the pore pressure, P. The vertical (lithostatic) stress, σ_z, is the greatest principal stress, σ_1, and least principal stress, σ_3, for the extensional (normal faulting) and compressional (thrust faulting) regimes, respectively. The mean stress is $\sigma_m = \frac{1}{2}(\sigma_1 + \sigma_3)$ and the radius, R, is half the stress difference, or $R = \frac{1}{2}(\sigma_1 - \sigma_3)$. For a crust pervasively fractured with faults of all orientations, $C \sim 0$, and failure will occur when the Mohr's circles for optimally oriented faults ($\theta = \theta_o$) first touch the Coulomb failure line, CFF=0. Intermediate stress regimes (dotted circle) ranging from transtensional through pure strike-slip to transpressional are represented by Mohr's circles with an intermediate mean stress, σ_{Sm}, with $\sigma_{Em} < \sigma_{Sm} < \sigma_{Cm}$. The small dashed circle illustrates case for super-hydrostatic pore pressure in an extensional regime. Hydrofracturing will result along vertically oriented cracks in the extensional regime if the pore pressure exceeds the least principal stress such that $\sigma_3 \leq 0$. (B) Schematic illustration of dynamic triggering in the Coulomb failure model in an extensional regime. The point $\mathbf{T}_1 = \mathbf{T}(R_1, \theta_1)$ represents a stable stress state slightly below the failure threshold on a fault at an angle θ_1 with respect to the local least principal stress direction, σ_3. At $t = t_0$ dynamic stresses from a distant earthquake arrive producing an oscillatory perturbation $\mathbf{T}(R(t), \theta(t))$ in both the orientation and magnitude of the local stress field. Slip occurs whenever $\mathbf{T}(R(t), \theta(t)$ inters the Coulomb failure zone, CFF ~ 0 (grey band) confining $\mathbf{T}(R(t), \theta(t))$ excursions to within or below this zone ($CFF \geq 0$). The dynamic stresses die away at time $t = t_d > t_0$, and the stress state on the fault settles to $\mathbf{T}_2 = \mathbf{T}(R_2, \theta_2)$ for $t > t_d$ reflecting the stress drop associated with the triggered seismicity. The greatest principal stress, σ_z , remains pinned to the lithostatic load in an extensional regime.

Figure 6. Examples of triggered seismicity detected within the surface wave coda from the Denali Fault earthquake at Mammoth Mountain. The top trace is a broadband seismogram, and the middle trace is a high-pass filtered version of the broadband record revealing the locally triggered activity as a spasmodic burst consisting of rapid-fire earthquakes. The bottom panel in is a spectrogram of the broadband seismogram from station OMM located 4 km southeast of Mammoth Mountain. Note the utility of the spectrogram display in revealing local earthquakes within the low-frequency coda as narrow vertical bands rich in high frequency energy. Modified from Prejean et al. (2004) courtesy of the Seismological Society of America.

Figure 7. (A) Map of triggered seismicity beneath Long Valley caldera and Mammoth Mountain for the Landers (green), Hector Mine (blue), and Denali Fault earthquakes (red). Modified from Prejean et al. (2004) courtesy of the

Seismological Society of America. Grey dots show seismicity for 1997-1998. The red circle centered on station OMM indicates area within which the Denali Fault-triggered earthquakes must be located based on S-P times. The singe red dot is the epicenter for the only of these earthquakes large enough for a multi-station location (Prejean et al. 2004). (B) Deformation transient triggered by the Landers earthquake as recorded on the POPA borehole dilatometer (top) and the long base tiltmeter, LBT. The bottom two panels show E-W and N-S tilt components, respectively. Cumulative number of earthquakes plotted in second panel. Adopted from Jonston et al. (1995) courtesy of the Seismological Society of America. (C) Deformation transient triggered by the Hector Mine earthquake as recorded on borehole dilatometers POPA, MCX, and BSP (Johnston et al. 2000). Cumulative number of earthquakes plotted in bottom panel. (D) Deformation transient triggered by the Denali Fault earthquake as recorded on borehole dilatometers POPA, MCX, and BSP. Strain records for each dilatometer are shown with solid Earth tides (top) and with tides filtered out (bottom). Cumulative number of earthquakes plotted in bottom panel. Adopted from Johnston et al.(2004a) courtesy of Seismological Society of America.

Figure 8. Seismic records showing the triggered response of Mt Wrangell, Alaska, to the dynamic waves from the 26 December 2004 M_W = 9.1 Sumatra-Andaman Islands earthquake from (West et al. 2005). (A) Short period vertical displacement seismogram of the Sumatra-Andaman Islands wavetrain at the summit station WANC at a distance of ~11,000 km from the epicenter. Time at top in hours, universal time. (B) Expanded view of highlighted section in (A) showing signal filtered with a band pass 0.5 to 20 Hz (top) and 0.01 to 0.1 Hz (bottom). (C) Spectrogram for the same time interval in (B). (D) comparison of WANC displacement seismograms with those from nearby stations. Dashed lines indicate a reference horizontal phase velocity of 3.1 km/sec. Reproduced with permission from *Nature.*

Notation and abbreviations

c	constant in Omori's law (equation 2)
C	cohesive strength in MPa
CFF	Coulomb failure function
ΔCFF	change in CFF
E	expected value
g	acceleration of gravity ms^{-1}
G	shear modulus, MPa
M	local magnitude
M_0	seismic moment
M_W	moment magnitude
MPa	mega Pascal
n_a	number of earthquakes in the interval t_a
n_b	number of earthquakes in the interval t_b
k	constant in Omori's law (equation 2)
K_1, K_2	constant values for CFF in Figure 5A
P	pore pressure
p	constant in Omori's law (equation 2)
R	Radius in Mohr's circle ½ ($\sigma_1 - \sigma_3$): see Figure 5A
t	time
t_0	origin time of distant mainshock or arrival time of dynamic stresses
t_a	specified time interval after t_0
t_b	specified time interval before t_0
Δt	time delay between t_0 and the onset of triggered seismicity
$\mathring{u}$	particle velocity
y	year
var	varance
v_s	phase velocity of a seismic shear wave
β	beta statistic
ε_p	peak dynamic strain
μ	coefficient of friction
δ	time increment used the beta statistic
Δ	epicentral distance, km
ρ	density
λ	mean recurrence time in a Poisson distribution
σ	effective stress component (σ_n - P)
σ_n	rock matrix stress component
σ_m	mean stress ½ ($\sigma_1 + \sigma_3$)
σ_1, σ_3	greatest and least principal stress components
σ_z	vertical principal stress
θ	angle between a fault plane and the least principal stress, σ_3
τ	shear stress component
T	traction acting on a fault plane at angle in Mohr's circle diagram (Figure 5B)
$\mathbf{T}_p$	peak dynamic stress

8:07 REFERENCES

Aagaard, B. T., Anderson, G. and Hudnut, K. W. 2004 Dynamic rupture modeling of the transition from thrust to strike-slip motion in the 2002 Denali Fault earthquake, Alaska *Bull. Seismol. Soc. America,* **94,** S190-S201.

Anderson, J. G., Brune, J. N., Louie, J. N., Zeng, Y., Savage, M., Yu, G., Chen, Q. and dePolo, D. 1994 Seismicity in the western Great Basin apparently triggered by the Landers, California, earthquake, 28 June 1992 *Bull. Seismol. Soc. America,* **84,** 863-891.

Anderson, O. L. and Grew, P. C. 1977 Stress corrosion theory of crack propagation with applications to geophysics *Reviews of Geophysics,* **15,** 77-104.

Antonioli, A., Cocco, M., Das, S. and Henery, C. 2002 Dynamic stress triggering during the great 25 March 1998 Antarctic Plate earthquake *Bull. Seismol. Soc. America,* **92,** 896-903.

Armstrong, B. H. and Stierman, D. J. 1989 Acoustic emissions from foreshocks and secular strain changes prior to earthquakes In *Acoustic emission/ microseismic activity in geologic structures and materials*, Vol. 17 (Ed, H. Reginald Hardy, J.) Trans Tech Publications, Pennsylvania State University, pp. 309-326.

Arnadottir, T., Geirsson, H. and Einarsson, P. 2004 Coseismic stress changes and crustal deformation on the Reykjanes Peninsula due to triggered earthquakes on 17 June 2000 *J. Geophys. Res.,* **109,** doi:10.1029/2004JB003130.

Atkinson, B. K. 1984 Subcritical crack growth in geological materials *J. Geophys. Res.,* **89,** 4077-4114.

Bagdassarov, N. 1994 Pressure and volume changes in magmatic systems due to the vertical displacement of compressible materials *J. Volcal. Geotherm. Res.,* **63,** 95-100.

Bakun, W. H. and McGarr, A. 2002 Differences in attenuation among stable contentenal regions *Geophysical Research Letters,* **29,** 36-1 to 36-4.

Beeler, N. M. and Lockner, D. A. 2003 Why earthquakes correlate weakly with the solid Earth tides: effects of periodic stress on the rate and probability of earthquake occurrence *J. Geophys. Res.,* **108,** doi:1029/2001JB001518.

Beresnev, I. A. and Wen, K.-L. 1995 Remotely triggered seismicity inferred from Taiwan regional catalog *Geophys. Res. Lett.,* **22,** 3155-3158.

Brodsky, E. E., 2006 Long-range triggered earthquakes that continue after the wave train passes *Geophys. Res. Lett*., **33**, doi: 10.1029/2006GL026605.

Brodsky, E., Sturtevant, B. and Kanamori, H. 1998 Earthquakes, volcanones, and rectified diffusion *J. Geophys. Res.,* **103,** 23,827-23-838.

Brodsky, E. E., Karakostas, V. and Kanamori, H. 2000 A new observation of dynamically triggered regional seismicity: earthquakes in Greece following the August, 1999, Izmit, Turkey earthquake *Geophys. Res. Lett.,* **27,** 2741-2744.

Brodsky, E. E. and Prejean, S. G. 2005 New constraints on mechanisms of remotely triggered seismicity at Long Valley Caldera *J. Geophys. Res.,* **110,** doi:10.1029/2004JB003211.

Brodsky, E. E., Roeloffs, E., Woodcock, D., Gall, I. and Manga, M. 2003 A mechanism for sustained groundwater pressure changes induced by distant earthquakes *J. Geophys. Res.,* **108,** doi:10.1029/2002JB002321.

Byerlee, J. D. 1980 Friction of rocks *Pure and Applied Geophysics,* **116,** 615-626.

Camelbeeck, T., van Eck, T., Pelzing, R., Ahorner, L., Loohuis, J., Haak, H. W., Hoang-Trong, P. and Hollnack, D. 1994 The 1992 Roermond earthquake, the Netherlands, and its aftershocks *Geologie en Mijnbouw,* **73,** 181-197.

Chouet, B. 1992 A seismic model for the source of long-period events and harmonic tremor In *Volcanic Seismology*(Eds, Gasparini, P., Scarpa, R. and Aki, K.) Springer-Verlag, Berlin, Heidelberg, New York, pp. 133-156.

Chouet, B., Dawson, P. and Nakano, M. in press Dynamics of diffusive bubble growth and pressure recovery in a bubbly rhyolitic melt embedded in an elastic solid *Journal of Geophysical Research*.

Christiansen, L., Hurwitz, S., Saar, M. O., Ingebritsen, S. E. and Hsieh, P. 2005 Seasonal seismicity at western United States volcanic centers *Earth Planet. Sci. Lett.,* **in press**.

Cocco, M. and Rice, J. R. 2002 Pore pressure and poroelasticity effects in Coulomb stress analysis of earthquake interactions *J. Geophys. Res.,* **107,** doi:10.1029/2002JB002319.

Cochran, E. S., Vidale, J. E. and Tanaka, S. 2004 Earth tides can trigger shallow thrust fault earthquakes *Science,* **306,** 1164-1166.

Das, S. and Scholz, C. 1981 Off-fault aftershock clusters caused by shear stress increase? *J. Geophys. Res*., **71**, 1669-1675.

Dieterich, J. H. 1979 Modeling of rock friction 1. Experimental results and constitutive equations *J. Geophys. Res.,* **84,** 2161-2168.

Eberhart-Phillips, D., Haeussler, P. J., Freymueller, J. T., Frankel, A. D., Rubin, C. M., Craw, P., Ratchkovski, N. A., Anderson, G., Carver, G. A., Crone, A. J., Dawson, T. E., Fletcher, H., Hansen, R., Harp, E. L., R.A., H., Hill, D. P., Hreinsdottir, S., Jibson, R. W., Jones, L. M., Kayen, R., Keffer, D. K., Larsen, C. F., S.C., M., Personius, S. F., Plafker, G., Sherrod, B., Sieh, K., Sitar, N. and Wallace, W. K. 2003 The 2002 Denali Fault earthquake, Alaska: a large magnitude, slip-partitioned event *Nature,* **300,** 1113-1118.

Emiliani, C., Harrison, C. G. A. and Swanson, M. 1969 Underground nuclear explosions and the control of earthquakes *Science,* **165,** 1255-1256.

Felzer, K. R. and Brodsky, E. E. 2005 Testing the stress shadow hypothesis *J. Geophys. Res.,* **110,** doi:10.1029/2004JB003277.

Felzer, K. R. and Brodsky, E. E. 2006 Evidence for dynamic aftershock triggering from earthquake densities *Nature* **441**, 735-738.

Fournier, R. O. 1999 Hydrothermal processes related to movement of fluid from plastic to brittle rock in the magmatic-epithermal environment *Economic Geology,* **94,** 1193-1211.

Freed, A. M. 2005 Earthquake triggering by static, dynamic, and postseismic stress transfer *Ann. Rev. Earth Planet. Sci.,* **33,** 335-367.

Galperin, E. I., Petersen, N. V., Sitnikov, A. V. and Vinnik, L. P. 1990 On the properties of short-period seismic noise *Physics of the Earth and Planetary Interiors,* **63,** 163-171.

Glowacka, E., Nava, A. F., Cossio, D. d., Wong, V. and Farfan, F. 2002 Fault slip, seismicity, and deformation in the Mexicali Valley, Baja California, Mexico, after the M 7.1 Hector Mine earthquake *Bull. Seismol. Soc. America,* **92,** 1290-1299.

Gomberg, J. 1996 Stress/strain changes and triggered seismicity following the Mw 7.3 Landers, California, earthquake *J. Geophys. Res.,* **101,** 751-764.

Gomberg, J., Blanpied, M. L. and Beeler, N. M. 1997 Transient triggering of near and distant earthquakes *Bull. Seismol. Soc. America,* **87,** 294-309.

Gomberg, J., Bodin, P., Larson, K. and Dragert, H. 2004 Earthquakes nucleated by transient deformations caused by the M=7.9 Denali, Alaska, earthquake *Nature,* **427,** 621-624.

Gomberg, J., Bodin, P. and Reasenberg, P. A. 2003 Observing earthquakes triggered in the near field by dynamic deformations *Bull. Seismol. Soc. America,* **93,** 118-138.

Gomberg, J. and Davis, S. 1996 Stress/strain changes and triggered seismicity at The Geysers, California *J. Geophys. Res.,* **101,** 733-749.

Gomberg, J. and Johnson, P. 2005 Dynamic triggering of earthquakes *Nature,* **437,** 830.

Gomberg, J., Reasenberg, P. A., Bodin, P. and Harris, R. 2001 Earthquakes triggering by seismic waves following the Landera and Hector Mine earthquakes *Nature,* **411,** 462-465.

Gomberg, J., Reasenberg, P. A., Cocco, M. and Belardinelli, M. E. 2005 A frictional population model of seismcity rate change *J. Geophys. Res.,* **110,** doi:10.1029/2004JB003404.

Green, H. W. I. 2003 Tiny triggers deep down *Nature,* **424,** 893-894.

Hainzl, S. and Ogata, Y. 2005 Detecting fluid signals in seismicity data through statistical earthquake modeling *Journal of Geophysical Research,* **110,** doi:10.1029/2004JBOO3247.

Hainzl, S., Sherbaum, F., and Beauval, C. 2006 Estimating background activity based on intervent-time distributions *Bull. Seismol. Soc. America*, **96**, 313-320.

Harrington, R. M. and Brodsky, E. E. 2006 The absence of remotely triggered seismicity in Japan *Bull. Seismol. Soc. America*, **96**, 871-878.

Harris, R. and Day, S. M. 1993 Dynamics of fault interaction: parallel strike-slip faults *J. Geophys. Res.,* **98,** 4461-4472.

Harris, R., Dolan, J. F., Hartlib, R. and Day, S. M. 2002 The 1999 Izmit, Turkey, earthquake: a 3-D dynamic stress transfer model of interearthquake triggering *Bull. Seismol. Soc. America,* **92,** 245-255.

Harris, R. A. 1998 Introduction to a special section: Stress triggers, stress shadows, and implications for seismic hazards *J. Geophys. Res.,* **103,** 24,347-24,358.

Hill, D. P. 1977 A model for earthquake swarms *J. Geophys. Res.,* **82,** 1347-1352.

Hill, D. P. in press Unrest in Long Valley Caldera, California: 1978-2004 In *Mechanisms of activity and unrest at large calderas*(Eds, De Natale, G., Troise, C. and Kilburn, C. R. J.) Geological Society of London, London.

Hill, D. P., Johnston, M. J. S., Langbein, J. O. and Bilham, R. 1995 Response of Long Valley Caldera to the Mw = 7.3 Landers, California, earthquake *Journal of Geophysical Research,* **100,** 12,985-13,005.

Hill, D. P., Pollitz, F. and Newhall, C. 2002 Earthquake-volcano interactions *Physics Today,* **55,** 41-47.

Hill, D. P., Reasenberg, P. A., Michael, A., Arabaz, W. J., Beroza, G., Brumbaugh, D., Brune, J. N., Castro, R., Davis, S., dePolo, D., Ellsworth, W. L., Gomberg, J., Harmsen, S., House, L., Jackson, S. M., Johnston, M. J. S., Jones, L., Keller, R., Malone, S., Munguia, L., Nava, S., Pechmann, J. C., Sanford, A., Simpson, R. W., Smith, R. B., Stark, M., Stickney, M., Vidal, A., Walter, S., Wong, V. and Zollweg, J. 1993 Seismicity remotely triggered by the magnitude 7.3 Landers, California, earthquake *Science,* **260,** 1617-1623.

Hough, S. E. 2001 Triggered earthquakes and the 1811-1812 New Madrid, central United States, earthquake sequence *Bull. Seismol. Soc. America,* **91,** 1547-1581.

Hough, S. E. 2005 Remotely triggered earthquakes following moderate mainshocks (or why California is not falling into the ocean) *Seismol. Res. Lett.,* **76,** 58-66.

Hough, S. E., Billham, R., Ambraseys, N. and Feldl, N. 2005 Revisiting the 1897 Shillong and 1905 Kangra earthquakes in northern India: site response, Moho reflections and a triggered earthquake *Current Science,* **88,** 1632-1638.

Hough, S. E. and Kanamori, H. 2002 Source properties of earthquakes near the Salton Sea triggered by the 16 October 1999 Mw 7.1 Hector Mine, California, earthquake *Bull. Seismol. Soc. America,* **92,** 1281-1289.

Hough, S. E., Seeber, L. and Armbruster, J. G. 2003 Intraplate triggered earthquakes: observations and interpretation *Bull. Seismol. Soc. America,* **93,** 2212-2221.

Hudnut, K.W.L., Seeber, L., and Pacheco, J. 1989 Cross-fault triggering in the November 1978 Superstition Hill earthquake sequence, southern California *Geophys. Res. Lett*., **16**, 199-202.

Husen, S., Taylor, R., Smith, R. B. and Healser, H. 2004a Changes in geyser eruption behavior and remotely triggered seismicity in Yellowstone National Park produced by the 2002 M 7.9 Delani fault earthquake, Alaska *Geology,* **32,** 537-540.

Husen, S., Wiemer, S. and Smith, R. B. 2004b Remotely triggered seismicity in the Yellowstone National Park region by the 2002 Mw 7.9 Denali Fault earthquake, Alaska *Bull. Seismol. Soc. America,* **94,** S317-S331.

Husker, A. L. and Brodsky, E. E. 2004 Seismcity in Idaho and Montana triggered by the Denali Fault earthquake: a window into the geologic context for seismic triggering *Bull. Seismol. Soc. America,* **94,** S310-S316.

Ichihara, M. and Brodsky, E.E. 2006 A limitation on the effect of rectified diffusion in volocanic systems *Geophysical Research Letters*, **33**, 10.1029/2005GL024733.

Johnson, P., Jai, X., and Gomberg, J. (submitted) The role of nonlinear dynamics in dynamic earthquake triggering, *J. Geophys. Res*.

Johnson, P. and Jia, X. 2005 Nonlinear dynamic, granular media and dynamic earthquake triggering *Nature,* **437,** 871-874.

Johnston, M. J., S,, Hill, D. P. and Pitt, A. M. 2000 Strain transient recorded in the Long Valley Caldera during triggered seismicity from the October 16, 1999 M7.1 Hector Mine, California, earthquake *Transactions of the American Geophysical Union, EOS,* **81,** WP1384.

Johnston, M. J., S,, Prejean, S. G. and Hill, D. P. 2004a Triggered deformation and seismic activity under Mammoth Mountain in Long Valley caldera by the 3 November 2002 Mw 7.9 Denali Fault earthquake *Bull. Seismol. Soc. America,* **94,** S360-S369.

Johnston, M. J. S., Hill, D. P., Linde, A. T., Langbein, J. and Bilham, R. 1995 Transient deformation during triggered seismicity from the 28 June 1992 Mw=7.3 Landers earthquake at Long Valley volcanic caldera, California *Bulletin of the Seismological Society of America,* **85,** 787-795.

Johnston, M. J. S., Prejean, S. and Hill, D. P. 2004b Triggered deformation and seismic activity in Long Valley Caldera by the November 3, 2002, M 7.9 Denali Fault Earthquake *Bulletin of the Seismological Society of America,* **94,** in press.

Julian, B. R. 1994 Volcanic tremor: nonlinear excitation by fluid flow *JGR,* **99,** 11,859-11,877.

Kanamori, H. and Brodsky, E. E. 2004 The physics of earthquakes *Reports in Progress in Physics,* **67,** 1429-1496.

Kilb, D., Gomberg, J. and Bodin, P. 2002 Aftershock triggering by complete Coulomb stress changes *J. Geophys. Res.,* **107,** doi:10.1029/2001JB000202.

King, G. C. P. and Cocco, M. 2001 Fault interactions by elastic stress changes: new clues from earthquake sequences *Advances in Geophysics,* **44,** 1-38.

King, G. C. P., Stein, R. S. and Lin, J. 1994 Static stress changes and the triggering of earthquakes *Bull. Seismol. Soc. America,* **84,** 935-953.

Kisslinger, C. and Jones, L. M. 1991 Properties of aftershock sequences in southern California *Journal of Geophysical Research,* **96,** 11,947-11,958.

Klein, F. W. 1976 Earthquake swarms and the semidiurnal solid earth tide *Geophysical Journal of the Royal Astronomical Society,* **45,** 245-295.

Lapusta, N., and Rice, J.R. 2003 Nucleation and early seismic propagation of small and large events in a crustal earthquake model, *J. Geophys. Res*., **108**, 10.1029/2001JB000793.

Lay, T., Kanamori, H., Ammon, C. J., Nettles, M., Ward, S. N., Aster, R. C., Beck, S. L., Brudzinski, M. R., Butler, R., DeShon, H. R., Ekstrom, G., Satake, K. and Sipkin, S. 2005 The great Sumatra-Andaman earthquake of 26 December 2004 *Science,* **308,** 1127-1132.

Linde, A. T. and Sacks, I. S. 1998 Triggering of volcanic eruptions *Nature,* **395,** 888-890.

Linde, A. T., Sacks, I. S., Johnston, M. J. S., Hill, D. P. and Billham, R. G. 1994 Increased pressure from rising bubbles as a mechanism for remotely triggered seismicity *Nature,* **371,** 408-410.

Lockner, D. A. and Beeler, N. M. 1999 Premonitory slip and tidal triggering of earthquakes *J. Geophys. Res.,* **104,** 20,133-20,151.

Lockner, D. A. and Beeler, N. M. 2002 Rock failure and earthquakes In *International Handbook of Earthquake and Engineering Seismology Part A*(Eds, Lee, W. H. K., Kanamori, H., Jennings, P. C. and Kisslinger, C.) Academic Press, Amsterdam, pp. 505-537.

Manga, M. and Brodsky, E. E. 2005 Seismic triggering of eruptions in the far field: volcanoes and geysers *Ann. Rev. Earth Planet. Sci.,* **in press**.

Mangan, M. and Sisson, T. 2000 Delayed, disequilibrium degassing in rhyolite magma: decompression experiments and implications for explosive volcanism *Earth and Planetary Science Letters,* **183,** 441-455.

Marsan, D. 2003 Triggering of seismicity at short distances following California earthquakes *J. Geophys. Res.,* **108,** doi:10.1029/2002JB001946.

Marzocchi, W. 2002 Remote seismic influence on large explosive eruptions *J. Geophys. Res.,* **107,** 10.1029/2001JB000307.

Matthews, M. V. and Reasenberg, P. A. 1988 Statistical methods for investigating quiescence and other temporal seismicity patterns *Pure and Applied Geophysics,* **126,** 357-372.

McGarr, A., Simpson, D. and Seeber, L. 2002 Case histories of induced and triggered seismicity In *International handbook of Earthquake and Engineering Seismology, Part A*(Eds, Lee, W. H. K., Kanamori, H., Jennings, P. C. and Kisslinger, C.) Academic Press, Amsterdam, pp. 647-664.

Meltzner, A. J. and Wald, D. J. 2003 Aftershocks and triggered events of the great 1906 California earthquake *Bull. Seismol. Soc. America,* **93,** 2160-2186.

Miyazawa, M., and Mori, J. 2006 Evidence suggesting fluid flow beneath Japan due to periodic seismic triggering from the 2004 Sumatra-Andaman earthquake, *Geophys. Res. Lett*., **33**, 10.1029/2005GL025087, L05303-L.

Miyazawa, M. and Mori, J. 2005 Detection of triggered deep low-frequency events from the 2003 Takachi-oki earthquake *Geophys. Res. Lett.,* **32,** L10307.

Miyazawa, M., Nakanishi, I., Sudo, Y. and Ohkura, T. 2005 Dynamic response of frequent tremors at Aso volcano to teleseismic waves from the 1999 Chi-Chi, Taiwan earthquake *J. Volcal. Geotherm. Res.,* **147,** 173-186.

Mohamad, R., Darkal, A. N., Seber, D., Sandoval, E., Gomez, F. and Barazangi, M. 2000 Remote earthquake triggering along the Dead Sea Fault in Syria following the 1995 Gulf of Aqaba earthquake (Ms=7.3) *Seismol. Res. Lett.,* **71,** 47-52.

Moran, S. C. 2003 Multiple seismogenic processes for high-frequency earthquakes at Katmai National Park, Alaska: evidence from stress tensor inversions of fault plane solutions *Bulletin of the Seismological Society of America,* **93,** 94-108.

Moran, S. C., Power, J. A., Stihler, S. D., Sanchez, J. J. and Caplin-Auerback, J. 2004 Earthquake triggering at Alaskan volcanoes following the 3 November 2002 Denali Fault earthquake *Bull. Seismol. Soc. America,* **94,** S300-S309.

Moran, S. C., Zimbelman, D. R. and Malone, S. D. 2000 A model for the magmatic-hydrothermal system at Mount Rainier, Washington, from seismic and geochemical observations *Bulletin of Volcanology,* **61,** 425-436.

Nicolaev, A. V. and Troitskii, P. A. 1987 Lithospheric studies based on array analysis of P-waves and microseisms *Tectonophysics,* **140,** 103-113.

Nur, A. and Booker, J. R. 1972 Aftershocks caused by pore fluid flow? *Science,* **175,** 885-887.

Obara, K. 2002 Nonvolcanic deep tremor associated with subduction in southwest Japan *Science,* **296,** 1679-1681.

Ogata, Y. 1993 Fast likelihood computation of epicemic type aftershock sequence model *Geophys. Res. Lett*. **20**, 2143-2146.

Omori, F. 1894 On the aftershocks of earthquakes *J. Coll. Sci. Imp. Univ. Tokyo,* **7,** 111-120.

Oppenheimer, D. H., Reasenberg, P. A. and Simpson, R. W. 1988 Fault plane solutions for the 1984 Morgan Hill, California, earthquake sequence: evidence for the state of stress on the Calavaras fault *Journal of Geophysical Research,* **93,** 9007-9026.

Pankow, K. L., Arabasz, W. J., Pechmann, J. C. and Nava, S. J. 2004 Triggered seismicity in Utah from the 3 November 2002 Denali Fault earthquake *Bull. Seismol. Soc. America,* **94,** S332-S347.

Perfettini, H. J., Schmittbuhl, J. and Cochard, A. 2003 Shear and normal load perturbations on a two-dimensional continuous fault: 2. dynamic triggering *J. Geophys. Res.,* **108,** doi:10.1029/2002JB001805.

Plafker, G. 1969 Tectonics of the March 27, 1964 Alaska earthquake *U.S. Geological Survey Prof. Paper* **543-I**, I1-I74.

Pollitz, F.F. and Johnston, M.J.S. 2006 Direct test of static stress versus dynamic stress triggering of aftershocks, Geophys. Res. Lett., 33, doi: 10:1029GL026764.

Pollitz, F. F. and Sacks, I. S. 2002 Stress triggering of the 1999 Hector Mine earthquake by transient deformation following the 1992 Landers earthquake *Bull. Seismol. Soc. America,* **92,** in press.

Power, J. A., Moran, S. C., McNutt, S. R., Stihler, S. D. and Sanchez, J. J. 2001 Seismic response of the Katmai volcanoes to the 6 December 1999 magnitude 7.0 Karlluk Lake earthquake, Alaska *Bull. Seismol. Soc. America,* **91,** 57-63.

Prejean, S. G., Hill, D. P., Brodsky, E. E., Hough, S. E., Johnston, M. J. S., Malone, S. D., Oppenheimer, D. H., Pitt, A. M. and Richards-Dinger, K. B. 2004 Remotely triggered seismicity on the United States west coast following the Mw 7.9 Denali Fault earthquake *Bull. Seismol. Soc. America,* **94,** S348-S359.

Pyle, D. M. and Pyle, D. L. 1995 Bubble migration and the initiation of volcanic eruptions *J. Volcal. Geotherm. Res.,* **67,** 227-232.

Reasenberg, P.A. Second-order moment of central California seismicity, 1969-1982 *J. Geophys. Res.* **90**, 5479-5479.

Reasenberg, P. A. and Simpson, R. W. 1992 Response of regional seismicity to the static stress change produced by the Loma-Prieta earthquake *Science,* **255,** 1,687-1,690.

Reinecker, J., Heidbach, O., Tingay, M., Connolly, P. and Muller, B. 2004 The 2004 release of the World Stress Map (available online at www.world-stress-map.org).

Rivera, L. and Kanamori, H. 2002 Spatial heterogeneity of tectonic stress in the crust *Geophysical Research Letters,* **39,** doi:10.1029/2001GL013803.

Roeloffs, E. 1996 Poroelastic techniques in the study of earthquake-related hydrologic phenomena *Advances in Geophysics,* **37,** 135-195.

Rowe, C., Christensen, D. and Carver, G. A. 2004 Preface to the issue dedicated to the 2002 Denali Fault earthquake sequence *Bulletin of the Seismological Society of America,* **94,** S1-S4.

Rybicki, K., Kato, T. and Kasahara, K. 1985 Mechanical interaction between neighboring active faults - static and dynamic stress field induced by faulting *Bulletin of the Earthquake Research Institute, Univeristy of Tokyo,* **60,** 1-21.

Sahagian, D. L. and Proussevitch, A. A. 1992 Bubbles in volcanic systems *Nature,* **359,** 485.

Sanchez, J. J. and McNutt, S. R. 2004 Intermediate-term declines in seismicity at Mt. Wrangell and Mt. Veniaminof volcanoes, Alaska, following the 3 November 2002 Mw 7.9 Denali Fault earthquake *Bull. Seismol. Soc. America,* **94,** S370-S383.

Savage, J.C., and Clark, M.M. 1982 Magmatic resurgence in Long Valley Caldera, eastern California, *Science*, **217**, 531-533.

Scholz, C. H. 1998 Earthquakes and friction laws *Nature,* **391,** 37-42.

Segall, P., Jonsson, S. and Agustsson, K. 2003 When is the strain in the rock the same as the strain in the rock? *Geophysical Research Letters,* **30,** doi:1029/2003GL017995.

Shapiro, S. A., Huenges, E. and Borm, G. 1997 Estimating the crust permeability from fluid-injection-induced seismic emission at the KTB site *Geophysical Journal International,* **131,** F15-F18.

.Shimomura, Y., Nishimura, T., and Sato, H. 2006, Bubble growth processes in magma surrounded by an elastic medium, *Jour. Volcanology and Geotherm. Res*., **155**, 307-322

Sibson, R. H. 1982 Fault zone models, heat flow, and the depth distribution of earthquakes in the continental crust of the United States *Bulletin of the Seismological Society of America,* **72,** 151-163.

Singh, S. K., Anderson, J. G. and Rodriguez, M. 1998 Triggered seismicity in the Valley of Mexico from major Mexican earthquakes *Geofiscia International,* **37,** 3-15.

Song, S.-R., Tsao, S. and Lo, H.-J. 2000 Characteristics of the Tatun volcanic eruptions, northern Taiwan; implications for a caldron formation and volcanic evolution *Journal of the Geological Society of China,* **43,** 361-378.

Spudich, P., Steck, L. K., Hellweg, M., Fletcher, J. B. and Baker, L. M. 1995 Transient stresses at Parkfield, California, produced by the M 7.4 Landers earthquake of June 28, 1992: observations from the UPSAR dense seismograph array *Journal of Geophysical Research,* **100,** 675-690.

Stark, M. A. and Davis, S. D. 1995 Remotely triggered microearthquakes at The Geysers geothermal field, California *Geophys. Res. Lett.,* **23,** 945-948.

Steacy, S., Gomberg, J. and Cocco, M. 2005 Introduction to special section: Stress transfer, earthquake triggering, and time-dependent seismic hazard *J. Geophys. Res.,* **110,** doi:10.1029/2005JB003692.

Steeples, D. W. and Steeples, D. D. 1996 Far field aftershocks of the 1906 earthquake *Bull. Seismol. Soc. America,* **86,** 921-924.

Stein, R. S. 1999 The role of stress transfer in earthquake occurrence *Nature,* **402,** 605-609.

Stein, R. S. and Lisowski, M. 1983 The 1979 Homestead Valley earthquake sequence, California: control of aftershocks and postseismic deformation *J. Geophys. Res.,* **88,** 6477-6490.

Stierman, D. J. 1977 A study of stress-dependent velocity variations *in situ* In *Department of Geophysics*Stanford University, Stanford, California.

Sturtevant, B., Kanamori, H. and Brodsky, E. 1996 Seismic triggering by rectified diffusion in geothermal systems *J. Geophys. Res.,* **101,** 25,269-25,282.

Tanaka, S., Ohtake, M. and Sato, H. 2004 Tidal triggering of earthquakes in Japan related to the regional tectonic stress *Earth, Planets, and Space,* **56,** 511-515.

Tibi, R., Wiens, D. A. and Inoue, H. 2003 Remote triggering of deep earthquakes in the 2002 Tonga sequence *Nature,* **424,** 921-925.

Tolstoy, M., Vernon, F. L., Orcutt, J. A. and Wyatt, F. K. 2002 Breathing of the seafloor: tidal correlations of seismcity at Axial volcano *Geology,* **30,** 503-506.

Ukawa, M., Fujita, E. and Kumagai, T. 2002 Remote triggering of microearthquakes at the Iwo-Jima volcano *Journal of Geography,* **111,** 277-286.

Vohis, R. C. 1967 *Hydrologic effects of the earthquake of March 27, 1964, outside Alaska,* U.S. Geological Survey, Washington D.C.

Voisin, C., Campillo, M., Ionescu, I. R., Cotton, F. and Scotti, O. 2000 Dynamic versus static stress triggering and friction parameters: inferences from the November 23, 1980, Irpinia earthquake *J. Geophys. Res.,* **105,** 21,647-21,658.

Voisin, C., Cotton, F. and Di Carli, S. 2004 A unified model for dynamic and static stress triggering of aftershocks, antishocks, remote seismicity, creep events, and multisegmented rupture *J. Geophys. Res.,* **109,** doi:10.1029/2003JB002886.

Wen, K.-L., Beresnev, I. A. and Cheng, S. 1996 Moderate-magnitude seismicity remotely triggered in the Taiwan Region by large earthquakes around the Philippine Sea Plate *Bull. Seismol. Soc. America,* **86,** 843-847.

West, M., Sanchez, J. J. and McNutt, S. R. 2005 Periodically triggered seismicity at Mount Wrangell, Alaska, after the Sumatra earthquake *Science,* **308,** 1144-1146.

Wiemer, S. 2001 A software package to analyze seismicity: ZMAP, *Seismol. Res. Lett*., **72**, 373-382.

Wiemer, S., and Wyss, M. 2000 Minimum magnitude of completeness in earthquake catalogs: examples from Alaska, the western United States, and Japan, *Bull. Seismol. Soc. America*, **90**, 859-869.

Zoback, M. D. and Zoback, M. L. 2002 State of stress in the Earth's lithosphere In *International Handbook of Earthquake and Engineering Seismology, Part A*(Eds, Lee, W. H. K., Kanamori, H., Jennings, P. C. and Kisslinger, C.) Academic Press, Amsterdam, pp. 559-568.

Ziv, A. 2006 On the role of multiple interactions in remote aftershock triggering: the Landers and the Hector Mine case studies *Bull. Seismol. Soc*. America, **96**, 80-89.

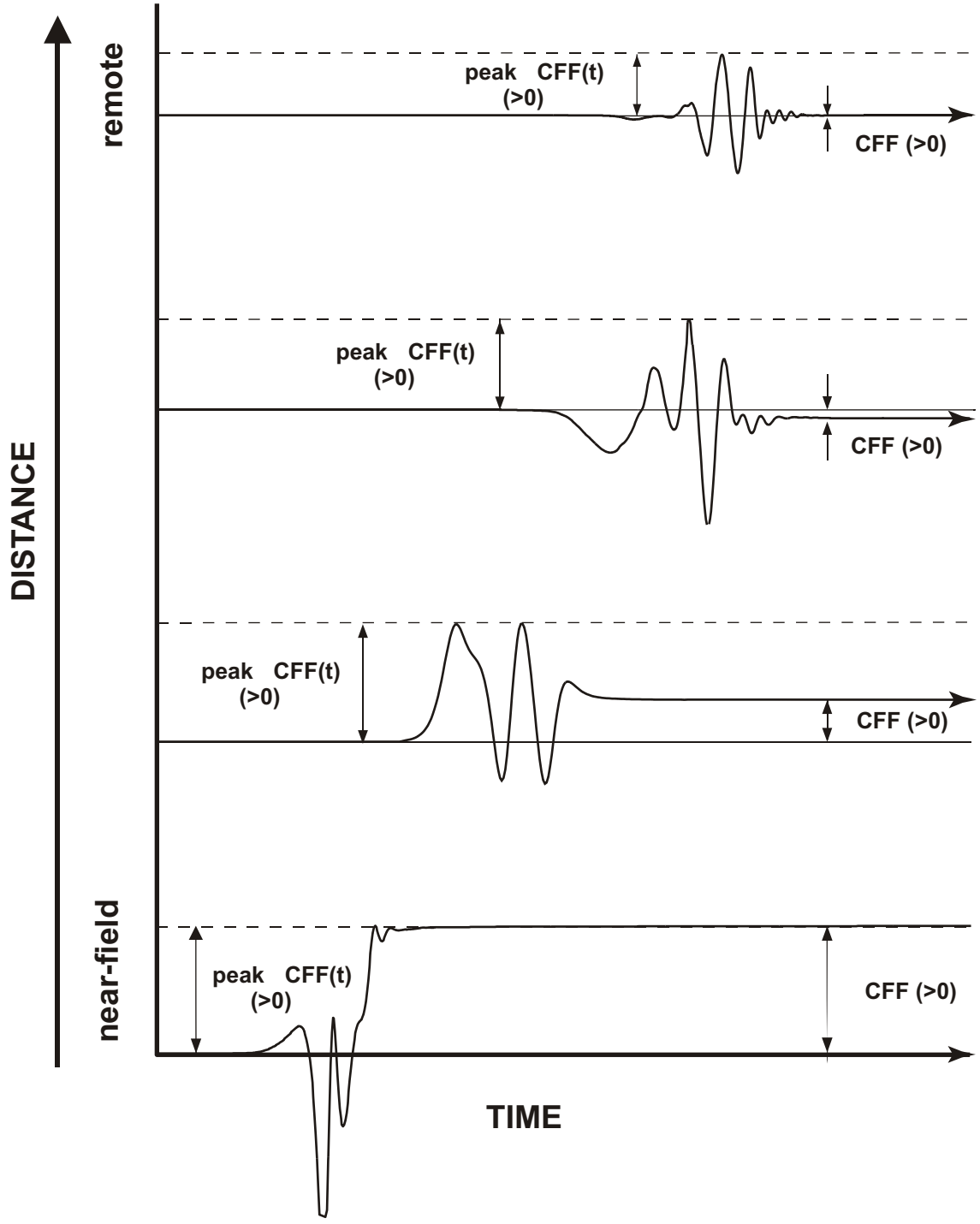
DISTANCE
remote
peak CFF(t)
(>0)
CFF (>0)
peak CFF(t)
(>0)
CFF (>0)
peak CFF(t)
(>0)
CFF (>0)
near-field
peak CFF(t)
(>0)
CFF (>0)
TIME

Fig. 1

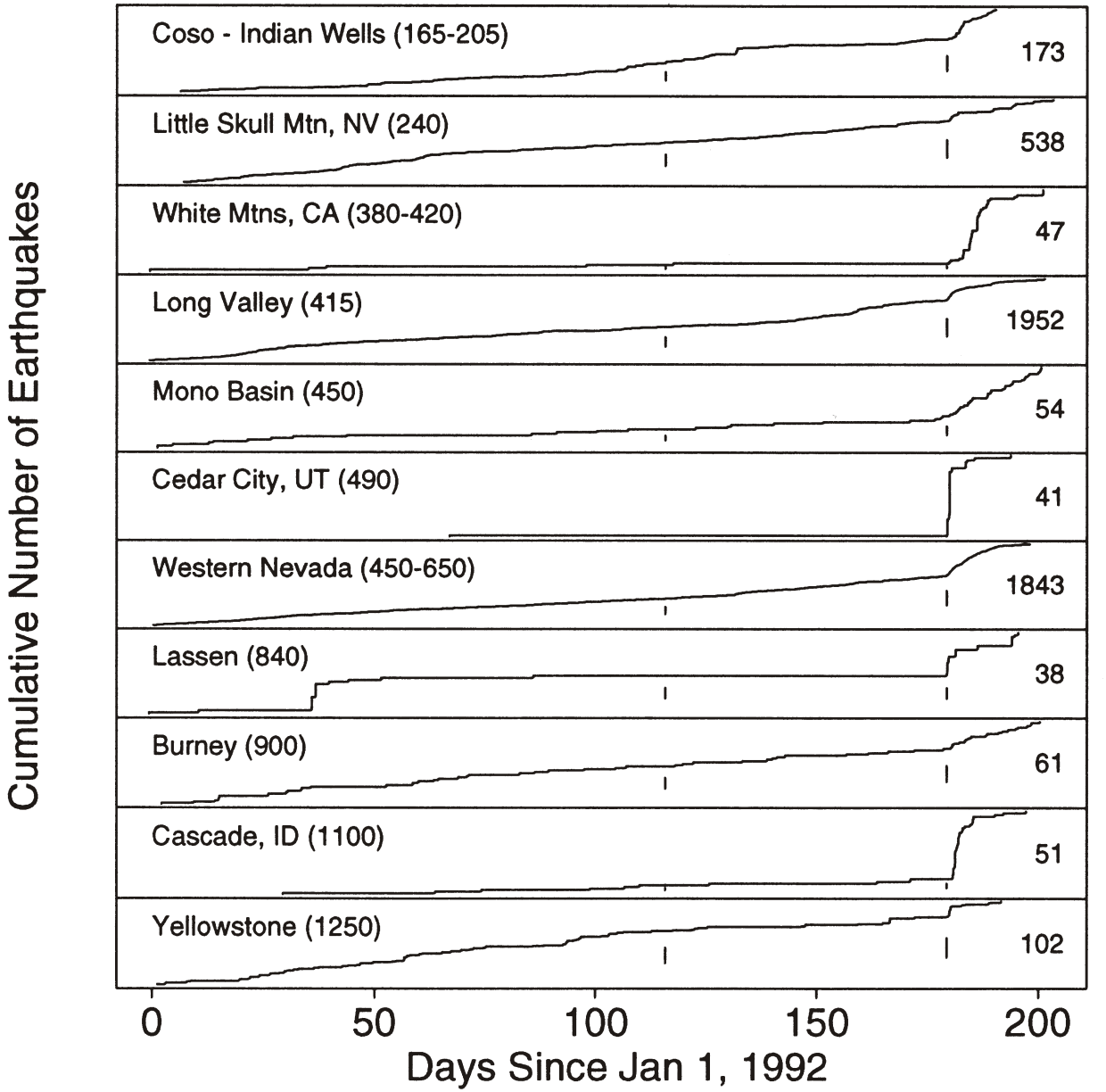
Cumulative Number of Earthquakes
Coso - Indian Wells (165-205)
173
Little Skull Mtn, NV (240)
538
White Mtns, CA (380-420)
47
Long Valley (415)
1952
Mono Basin (450)
54
Cedar City, UT (490)
41
Western Nevada (450-650)
1843
Lassen (840)
38
Burney (900)
61
Cascade, ID (1100)
51
Yellowstone (1250)
102
0
50
100
150
200
Days Since Jan 1, 1992

Fig 2

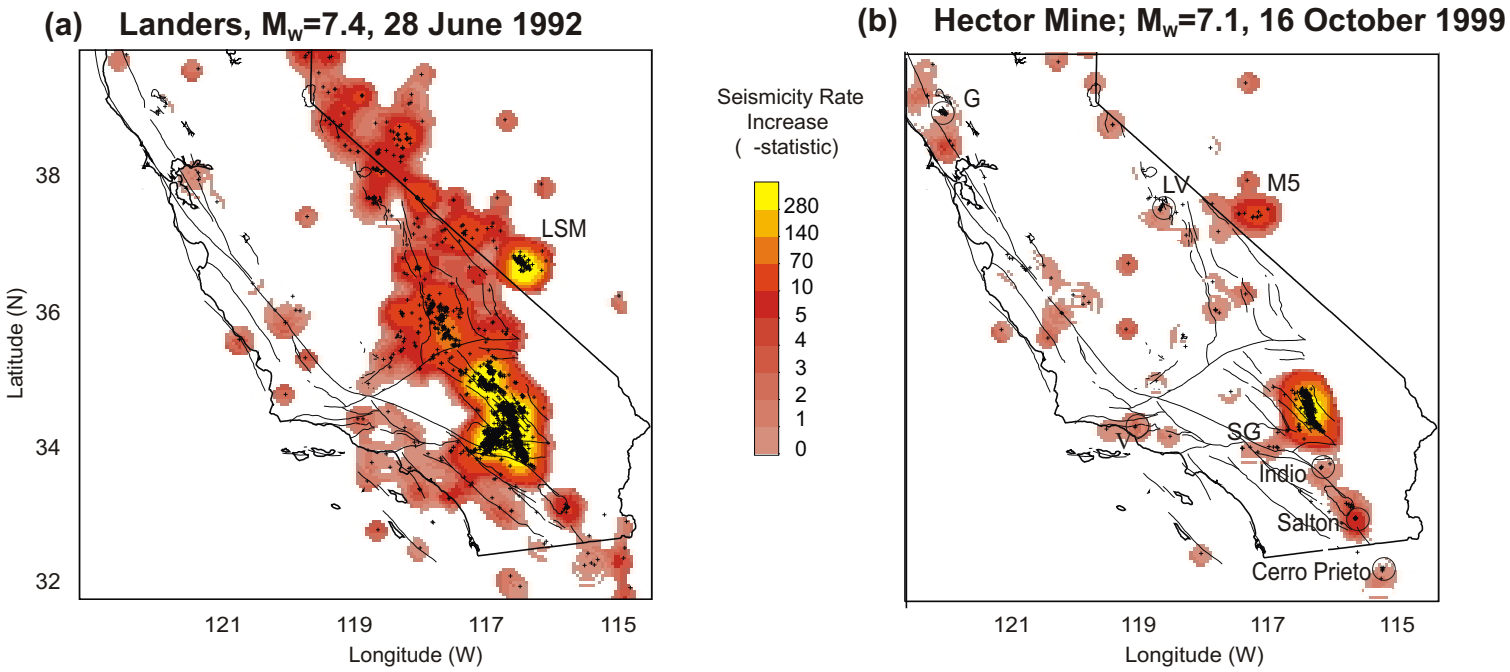
(a) Landers, M_w=7.4, 28 June 1992
LSM
Latitude (N)
38
36
34
32
121
119
117
115
Longitude (W)
Seismicity Rate Increase (-statistic)
280
140
70
10
5
4
3
2
1
0
(b) Hector Mine; M_w=7.1, 16 October 1999
G
LV
M5
SG
Indio
Salton
Cerro Prieto
121
119
117
115
Longitude (W)

Figure 3

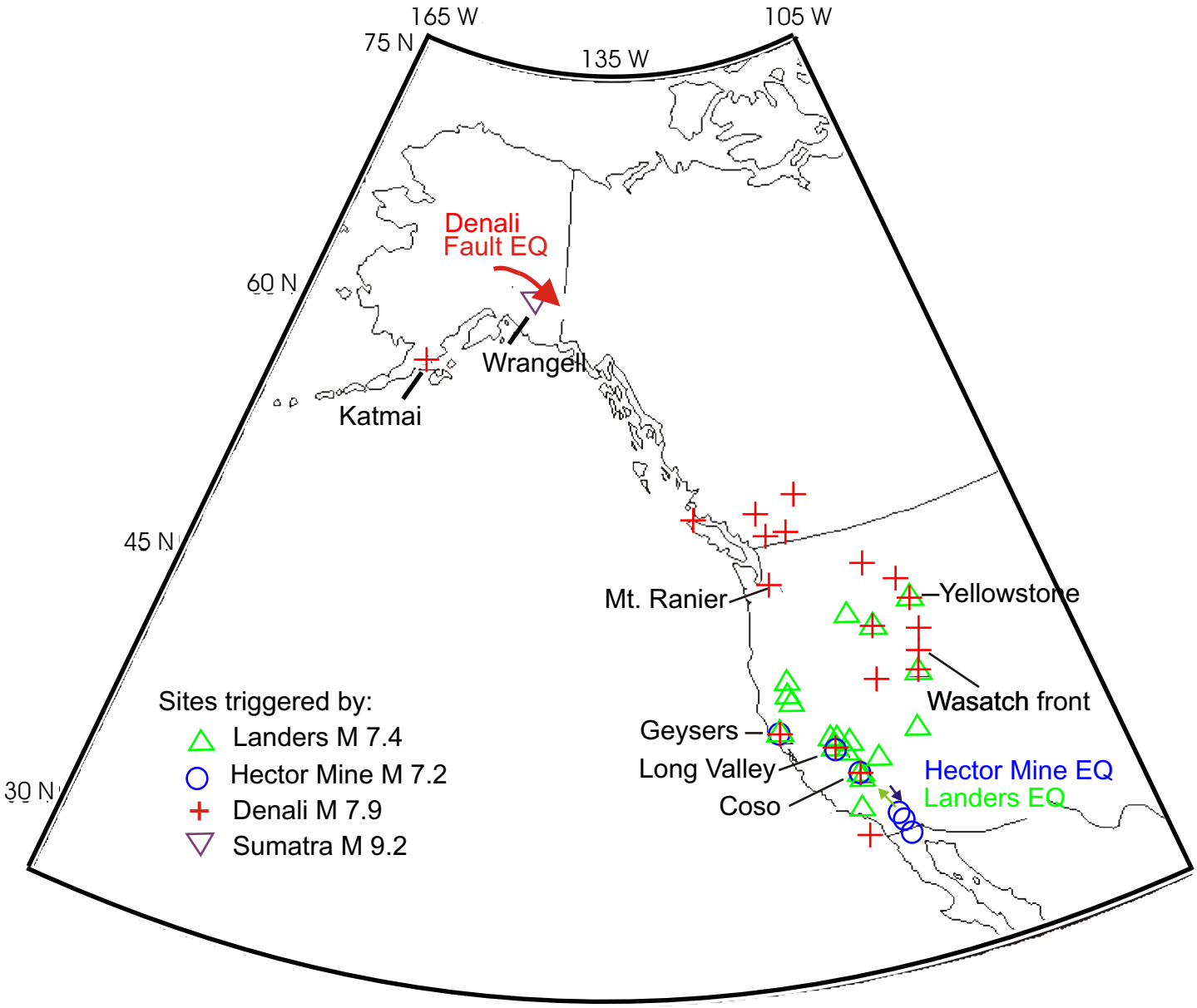
165 W
105 W
75 N
135 W
Denali
Fault EQ
60 N
Wrangell
Katmai
45 N
Mt. Ranier
Yellowstone
Wasatch front
Geysers
Long Valley
Coso
Hector Mine EQ
Landers EQ
30 N
Sites triggered by:
Landers M 7.4
Hector Mine M 7.2
Denali M 7.9
Sumatra M 9.2

Fig. 4

A

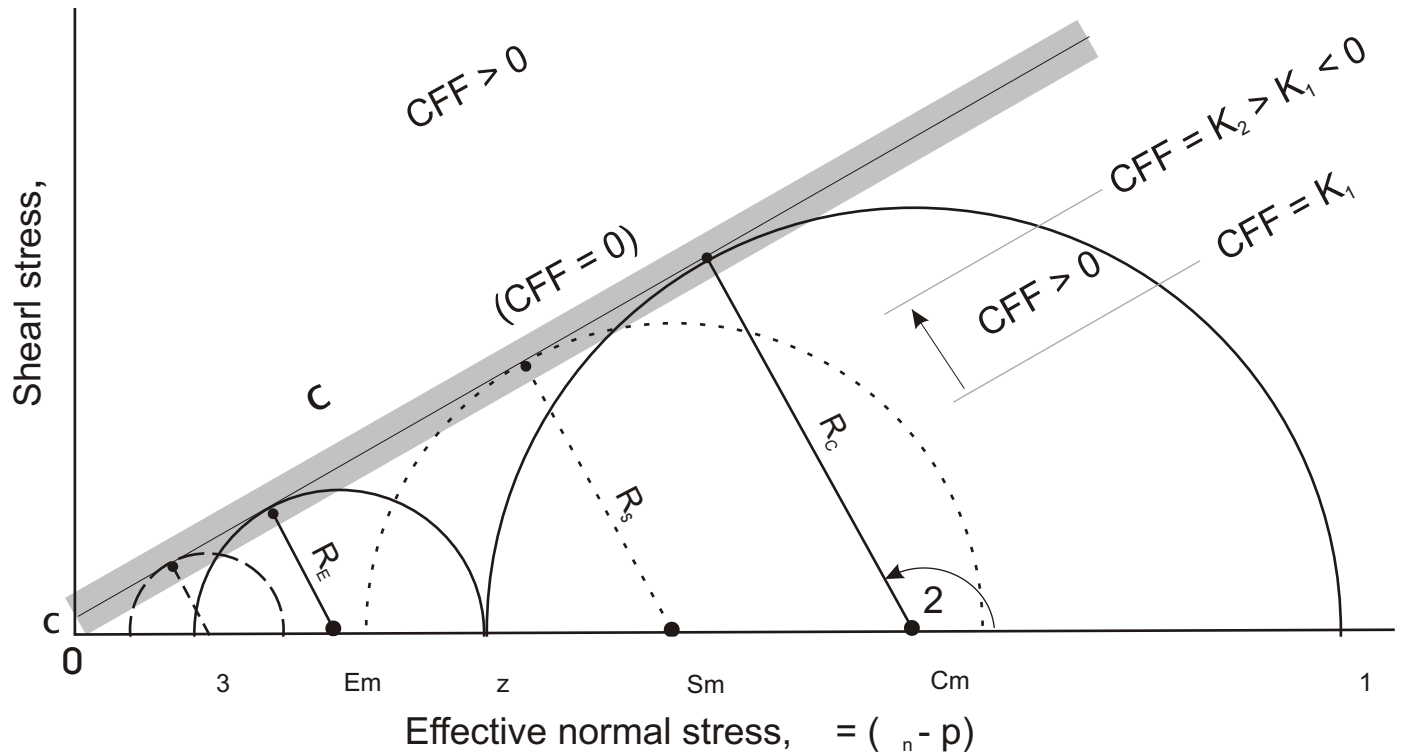
CFF > 0
(CFF = 0)
CFF = K2 > K1 < 0
CFF = K1
CFF > 0
Shearl stress,
c
c
0
3
Em
z
Sm
Cm
1
2
Effective normal stress, = (n - p)
Extensional
Normal
Strike-slip
Compressional
Thrust

Fig 5A

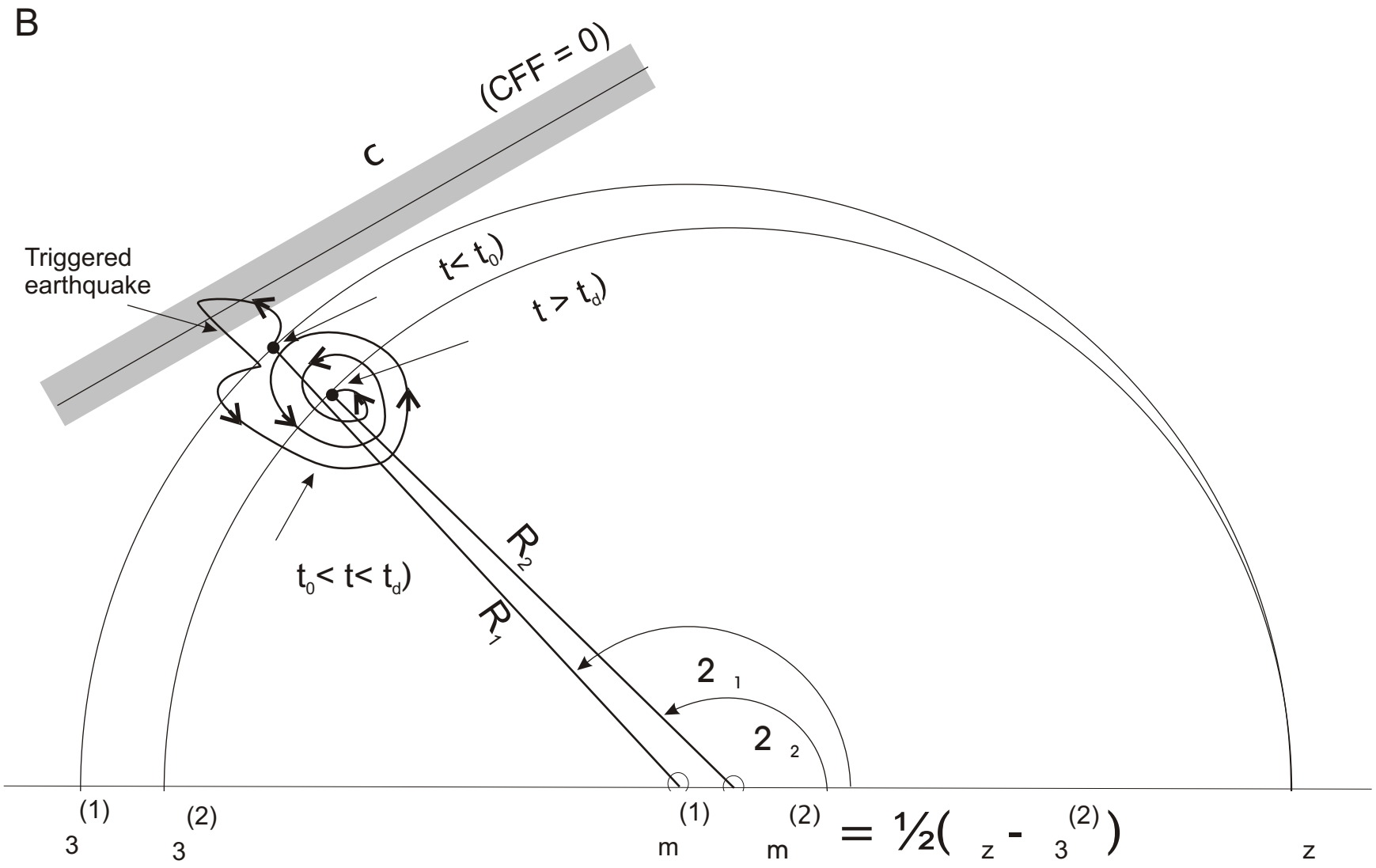
B
(CFF = 0)
c
Triggered
earthquake
t< t0)
t > td)
t0< t< td)
R2
R1
2 1
2 2
(1)
3
(2)
3
(1)
m
(2)
m
= ½(z - 3 (2))
z
Effective normal stress, = (n - p)

Fig 5B

M 7.9 Denali Fault Earthquake Triggered Seismicity at Mammoth Mt., California

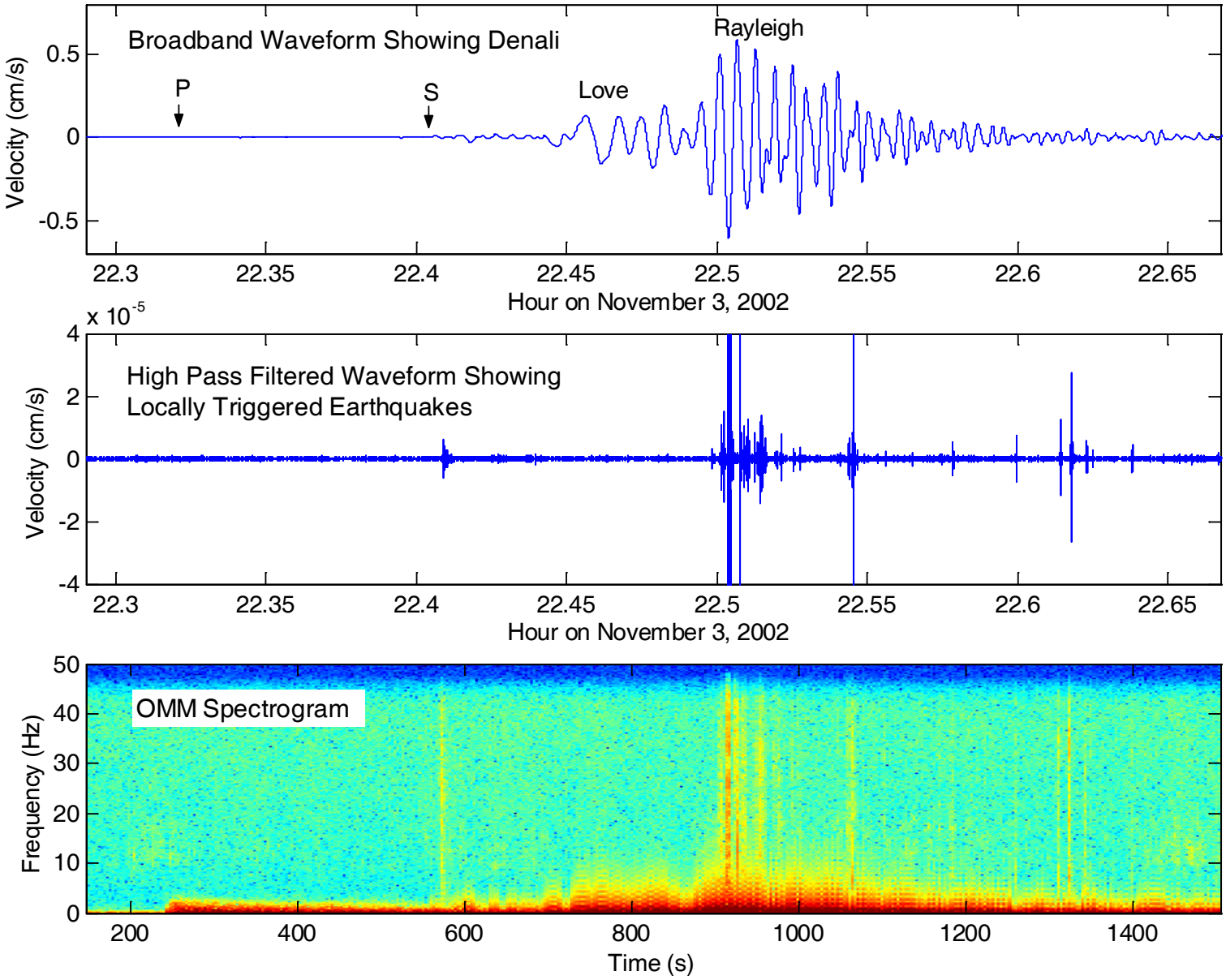

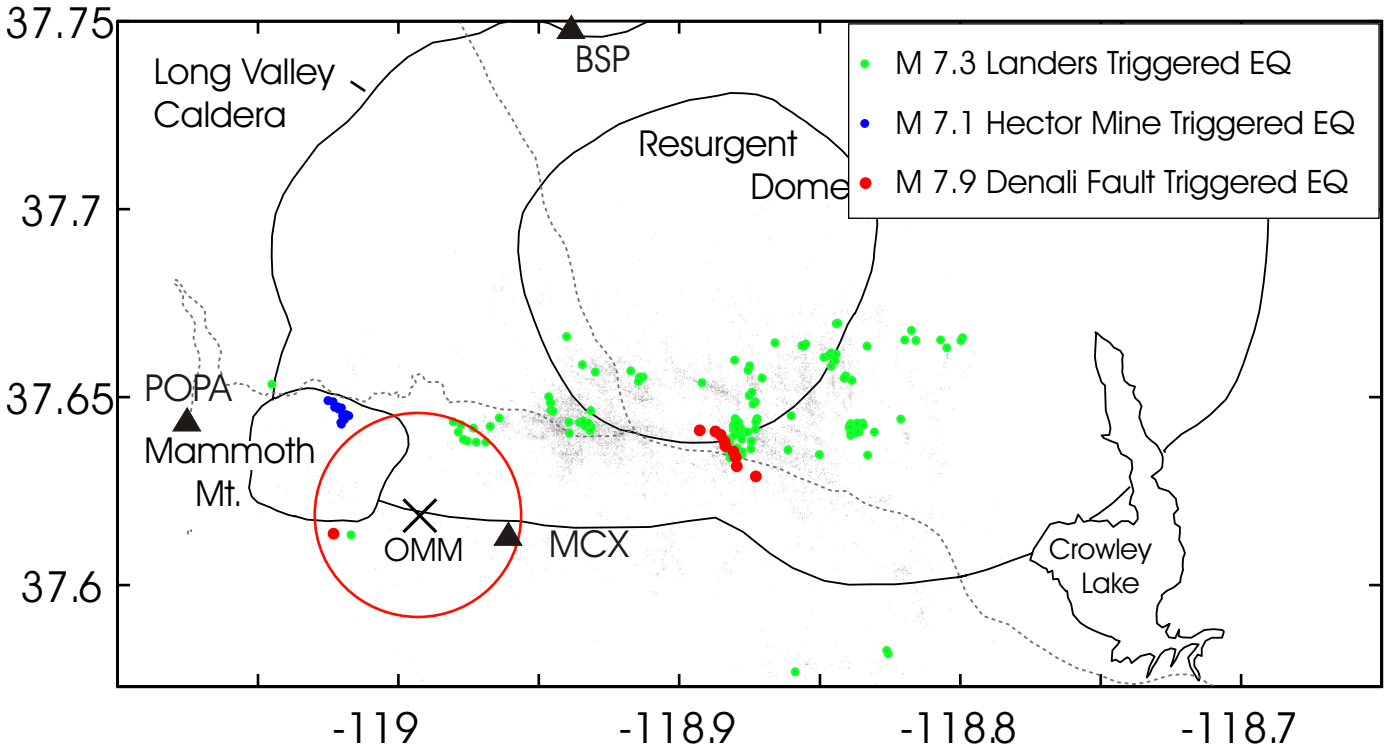

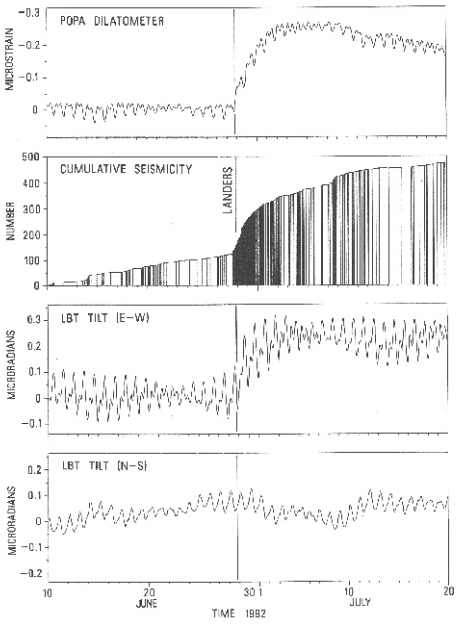

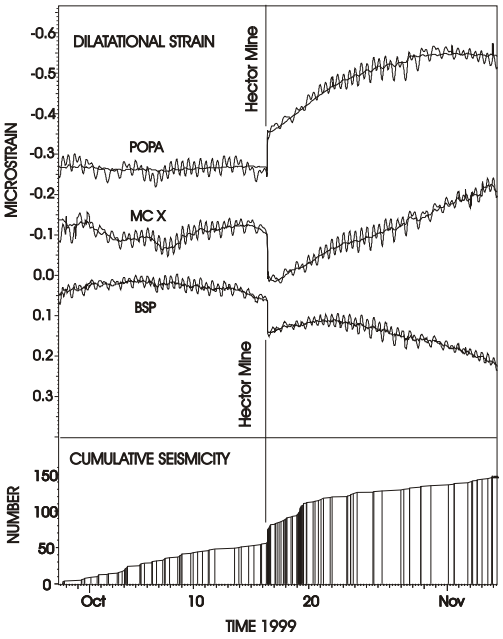

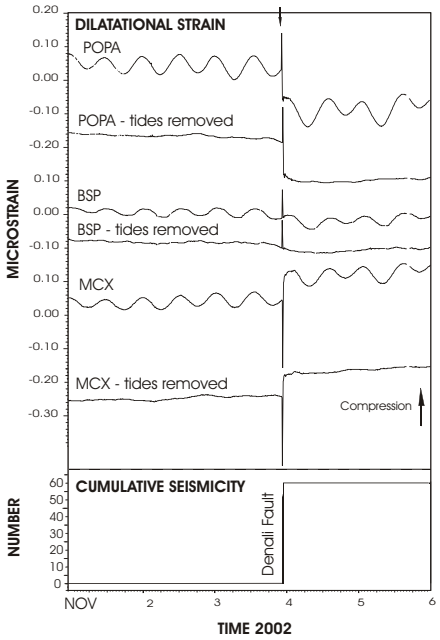

Landers M=7.4
D = 438 km

Hector Mine M=7.1
D = 397 km

Denali Fault M=7.9
D = 3,454 km

Fig 7

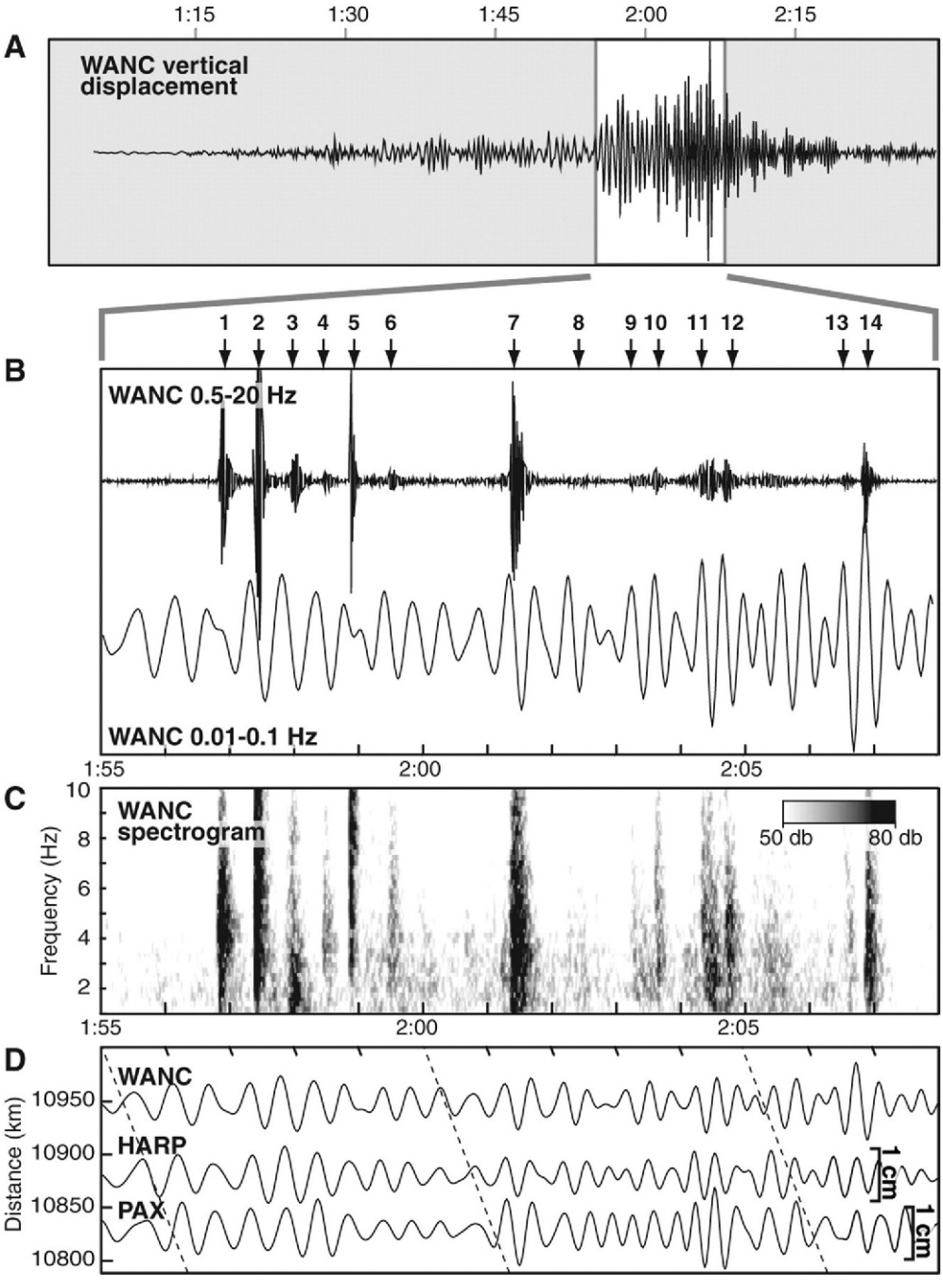
A
1:15
1:30
1:45
2:00
2:15
WANC vertical displacement
B
1 2 3 4 5 6 7 8 9 10 11 12 13 14
WANC 0.5-20 Hz
WANC 0.01-0.1 Hz
1:55
2:00
2:05
C
WANC spectrogram
50 db
80 db
Frequency (Hz)
10
8
6
4
2
1:55
2:00
2:05
D
WANC
HARP
PAX
Distance (km)
10950
10900
10850
10800
1 cm
1 cm